energies

MDPI

Article

Comparison of Catalytic Activity of ZIF-8 and Zr/ZIF-8 for Greener Synthesis of Chloromethyl Ethylene Carbonate by CO_2 Utilization

Bisi Olaniyan and Basudeb Saha *

School of Engineering, London South Bank University, 103 Borough Road, London SE1 0AA, UK; olaniyab@lsbu.ac.uk

* Correspondence: b.saha@lsbu.ac.uk; Tel.: +44-(0)20-7815-7190; Fax: +44-(0)20-7815-7699

Received: 26 November 2019; Accepted: 15 January 2020; Published: 21 January 2020

Abstract: The catalytic activity of both ZIF-8 and Zr/ZIF-8 has been investigated for the synthesis of chloromethyl ethylene carbonate (CMEC) using carbon dioxide (CO_2) and epichlorohydrin (ECH) under solvent-free conditions. Published results from literature have highlighted the weak thermal, chemical, and mechanical stability of ZIF-8 catalyst, which has limited its large-scale industrial applications. The synthesis of novel Zr/ZIF-8 catalyst for cycloaddition reaction of ECH and CO_2 to produce CMEC has provided a remarkable reinforcement to this weak functionality, which is a significant contribution to knowledge in the field of green and sustainable engineering. The enhancement in the catalytic activity of Zr in Zr/ZIF-8 can be attributed to the acidity/basicity characteristics of the catalyst. The comparison of the catalytic performance of the two catalysts has been drawn based on the effect of different reaction conditions such as temperature, CO_2 pressure, catalyst loading, reaction time, stirring speed, and catalyst reusability studies. Zr/ZIF-8 has been assessed as a suitable heterogeneous catalyst outperforming the catalytic activities of ZIF-8 catalyst with respect to conversion of ECH, selectivity and yield of CMEC. At optimum conditions, the experimental results for direct synthesis of CMEC agree well with similar literature on Zr/MOF catalytic performance, where the conversion of ECH, selectivity and the yield of CMEC are 93%, 86%, and 76%, respectively.

Keywords: ECH; epichlorohydrin; CMEC; chloromethyl ethylene carbonate; CO_2; carbon dioxide; MOF; metal organic framework; ZIF-8; zeolitic imidazolate framework; Zr/ZIF-8; zirconium/zeolitic imidazolate framework

1. Introduction

The effective transformation and utilization of anthropogenic carbon dioxide (CO_2) is a subject of political and environmental debates in recent years, which have been actively pursued by the academia and energy industries in order to promote a sustainable environment [1]. The current level and accumulation of CO_2 in the atmosphere is high and requires urgent attention [2]. However, regardless of environmental regulations and discharge limits placed on greenhouse gases emitted into the atmosphere, CO_2 is believed to be environmentally benign, abundant, nontoxic, non-flammable, and a readily available C1 source for the synthesis of organic carbonate [3]. Therefore, the synthesis of cyclic organic carbonates *via* the cycloaddition of CO_2 and epoxides is one of the most promising reaction schemes because of its 100% atom efficiency [4]. Cyclic organic carbonates such as chloromethyl ethylene carbonate (CMEC), propylene carbonate (PC), styrene carbonate (SC), and ethylene carbonate (EC) are widely used as polar aprotic solvents, electrolytes for lithium-ion batteries, automobile, cosmetic, fuel additives materials, alkylating and carbonylating reagents, and fine chemicals for pharmaceuticals [5,6].

In the past two decades, several attempts have been made to develop greener and sustainable catalytic systems for chemical fixation of CO_2. This includes conventional solid catalysts such as zeolites, salen Cr(III) complexes, metal oxides, quaternary ammonium salts, polymer-supported catalysts, ionic liquids (ILs), etc. However, these attempts have failed to yield satisfactory results as most of these catalysts require high temperature and/or pressure (usually around 453 K and pressure higher than 8 atm), further separation and purification steps, and low product yield [7]. This is uneconomical from a commercial point of view and hence, the research has been directed to employ a novel catalyst that provides solutions to all these shortfalls i.e., metal organic framework (MOF). Although, microporous materials such as zeolites, crystalline aluminosilicate, activated carbon, etc. have been known for their high surface area and high porosity, however, their applications have been limited especially in the field of heterogeneous catalysis due to difficulty in pore modification [7].

Metal organic framework (MOF) catalysts are identified as multidimensional porous polymetric crystalline organic-inorganic hybrid materials with exceptional characteristics including an ultrahigh specific surface area, enormous pore spaces, and ordered crystalline structure [8]. MOFs have emerged as a suitable candidate for the synthesis of organic carbonates from CO_2 and epoxide due to their unique heterogeneity and reusability requirements [9]. MOF-based catalysts often display higher catalytic activity than their corresponding homogenous catalysts as evidenced in many catalytic reactions such as ring opening, addition reactions, oxidation reactions, hydrogenation and isomerization [10]. Zeolitic imidazolate frameworks, (ZIFs), is one of the subclasses of MOFs with a similar structure to zeolites. It has attractive structural properties and intrinsically lower density. Many experiments involving ZIF-8 have shown great applications in multidisciplinary fields such as catalysis, drug deliveries, purification and gas storage [11].

Recently, the stability of MOFs for large-scale industrial applications has been questioned in many published papers [11–15]. This is due to their weak thermal, chemical, and mechanical stability due to the structure of inorganic bricks and the nature of the chemical bonds they form with the linker [15]. In order to improve this weak thermal functionality and gain in-depth knowledge of their catalytic activities, Cavka et al. [16] was the first group to synthesize Zr-based MOFs designated as zirconium 1,4-dicarboxybenzene, UiO-66 for photocatalysis [17]. The test conducted by the group found that the increased stability of the Zr-based MOFs is owing to the Zr-O bonds formed between the cluster and carboxylate ligands [18]. Several other groups have thereafter explored this opportunity, which has seen the increased application of Zr-based MOFs in many research activities. Demir et al. [19] utilized UiO (University of Oslo) type zirconium metal–organic frameworks in a solvent-free coupling reaction of carbon dioxide (CO_2) and epichlorohydrin (ECH) for the synthesis of epichlorohydrin carbonate (ECHC). The results of their experiments have increased the use of zirconium-based (Zr-based) MOFs for the catalytic synthesis of organic carbonates from CO_2 and epoxides.

From our experiments, the synthesis of Zr-doped MOF (Zr/ZIF-8) for the cycloaddition reaction of CO_2 and ECH in the synthesis of chloromethyl ethylene carbonate (CMEC) has demonstrated reasonable thermal stability under relatively mild reaction conditions without using any solvent or co-catalyst. Although, the synthesis of several Zr-based MOFs have been reported in recent times (albeit in early stages), only a few were employed for catalytic studies even more rarely for the synthesis of organic carbonates from CO_2 and epoxides. Zr-based MOFs have exhibited increased structural tailorability as a result of the organic linkers in the catalyst frameworks [19].

Zirconium-based MOFs have demonstrated proof-of-concept applications in several areas such as toxic analyte, catalysis, gas storage, *vivo* drug delivery, and bio-sensing [20]. In this paper, a novel Zr/ZIF-8 has been successfully synthesized using the conventional solvothermal method. The prepared catalyst has been assessed as an innovative greener and sustainable heterogeneous catalyst for the direct synthesis of CMEC from CO_2 and ECH. The effect of various reaction parameters has been investigated and critically analyzed. These include the effect of reaction time, catalyst loading, temperature, CO_2 pressure, and stirring speed. Catalyst reusability studies of Zr/ZIF-8 was also investigated to establish its stability and reusability for the synthesis of CMEC.

2. Experimental Methods

2.1. Chemicals and Materials

Acetone (99%), chloromethyl ethylene carbonate (99%), epichlorohydrin (purity; 99%), zinc nitrate hexahydrate ($Zn(NO_3)_2{\cdot}6H_2O$ (purity; 99%), dimethylformamide (purity; 99%), and zirconium (IV) oxynitrate hydrate ($ZrO(NO_3)_2{\cdot}6H_2O$, 99.99%) were purchased from Sigma-Aldrich Co. LLC, Dorset, UK. Methanol (99%) and *n*-pentane 99.8%) were both procured from Fisher Scientific UK Ltd, Loughborough, UK. ZIF-8 catalyst was purchased from Sigma-Aldrich Co. LLC under the trademark of Basolite Z1200. All chemicals and catalysts were used without further purification or pre-treatment.

2.2. Catalysts Preparation

Preparation of ZIF-8 and zirconium-doped ZIF-8 (Zr/ZIF-8) were synthesized according to a method, which was previously described elsewhere [20,21]. Briefly, 8 mmol of zinc nitrate hexahydrate ($Zn(NO_3)_2{\cdot}6H_2O$ 99.99%) and zirconium (IV) oxynitrate hydrate ($ZrO(NO_3)_2{\cdot}6H_2O$, 99.99%) solutions in a stoichiometric ratio of Zn:Zr = 10:0 and Zr:Zn = 9:1 (to synthesis ZIF-8 and Zr/ZIF-8 respectively) were dissolved in 6.2 mmol of methanol. A separate solution of 14.2 mmol of 2-methylimidazole and 600 mml of methanol was prepared in another flask, which was added by dropwise addition to the Zr–Zn-based solution. The mixture conducted in an ambient temperature under nitrogen flow was vigorously stirred for 6 h. The Zr-doped ZIF-8 crystals were collected and separated by centrifugation at 300 rpm for 30 min. The solution was washed thoroughly with methanol three times and then dried at room temperature conditions. The crystals were left to dry overnight at 373 K. The greyish-white powders of Zr–ZIF-8 samples were further washed with DMF for 24 h in order to remove any excess of an unreacted organic linker. The solution was then heated at a temperature of 373 K in order to activate it. The samples were allowed to cool to room temperature naturally before being capped in a vial and refrigerated, ready for use in catalytic reactions. The obtained samples were identified with a stoichiometric ratio of Zr:Zn = 10:0 and Zr:Zn = 1:9 for ZIF-8 and Zr/ZIF-8 respectively.

2.3. Experimental Procedure for the Synthesis of Chloromethyl Ethylene Carbonate (CMEC)

In a typical cycloaddition reaction, a 25 mL stainless steel high-pressure reactor was initially charged with a specific amount of Zr/ZIF-8 catalyst and the limiting reactant, epichlorohydrin. A desired temperature was set on the reactor's panel controller; the reactor was then sealed and stirred continuously at a known stirring speed. At the desired temperature, a specific amount of liquid CO_2 was charged through a supercritical fluid (SCF) pump into the reactor. The reaction was left for the desired reaction time. After the reaction was completed, the reactor was cooled down to room temperature and the mixture was collected and filtered. The catalyst was separated, washed with acetone, and dried in a vacuum oven. A known amount of methanol (used as internal standard) was added to the product and analyzed using a gas chromatograph (GC). The effect of different reaction parameters was investigated. These include catalyst loading, stirring speed, CO_2 pressure, temperature, and reaction time. Reusability studies of both catalysts were also carried out in order to investigate the stability of the catalysts for the synthesis of chloromethyl ethylene carbonate.

2.4. Method of Analysis

A specific quantity of internal standard, methanol added to a known sample of the product was analyzed using a gas chromatography (GC) (Model: Shimadzu GC-2014). The stationary phase was a capillary column with dimensions (30 m length, 320 μm inner diameter, and 0.25 μm film thickness). Oxygen (99.9%) and hydrogen (99.9%) were used as ignition gases. The carrier gas used for the mobile phase was a high purity helium (99.9%) with a flow rate maintained at 1 mL min^{-1}. A temperature program was developed for the system where both the injector port and detector temperatures were kept isothermally at 523 K. The other selected program includes split ratio of 50:1 and injection volume of 0.5 μL. The column temperature was initially maintained at 323 K for 5 min, then followed by a

temperature ramp at a flow rate of 50 K min^{-1} to a temperature of 523 K with a 12 min run for each subsequent samples. The chromatogram shows that ECH peak at ~3.5 min, methanol at ~3.8 min, CMEC at ~11 min.

2.5. Proposed Reaction Mechanism

The proposed reaction mechanism involves two steps:

- The ring-opening of epoxides by a catalyst;
- Incorporation of carbon dioxide into the opening to form the cyclic carbonate.

The coupling reaction of CO_2 with epoxides can be initiated by activating either the epoxide or CO_2 or both at the same time [22]. This reaction, using a suitable heterogeneous catalyst, produces desired organic carbonates along with other side products. Figure 1 shows reaction pathways 1, 2, and 3 with corresponding products being chloromethyl ethylene carbonate, 3-chloropropane 1,2-diol, and 2,5-bis (chloromethyl)-1,4-dioxane respectively. The epoxide is activated when the oxygen atom interacts with the Lewis acid, this is then followed by a nucleophilic attack that provokes the opening of the epoxide ring [23] as shown in Figure 2. The activation of CO_2 can occur both through a nucleophilic attack with the oxygen atom as a nucleophile or an electrophilic attack with the carbon atom as an electrophile [24]. Figure 2 shows a proposed reaction mechanism for the synthesis of CMEC, where R is an alkyl group, A is a metal atom with a Lewis acid site, while B is an oxygen atom with a Lewis basic site. Zr/ZIF-8 is a dual-functional catalyst, which contains both the acidic and basic sites that are associated with the Lewis acid Zn^{2+} ions and the basic imidazole groups, respectively. The by-products identified with the coupling reaction of CO_2 and ECH as identified by the GC analysis are 3-chloropropane 1,2-diol and 2,5-bis (chloromethyl)-1,4-dioxane (see Figure 1). Figure 3 shows the schematic representation of the reaction of CO_2 and ECH to produce CMEC.

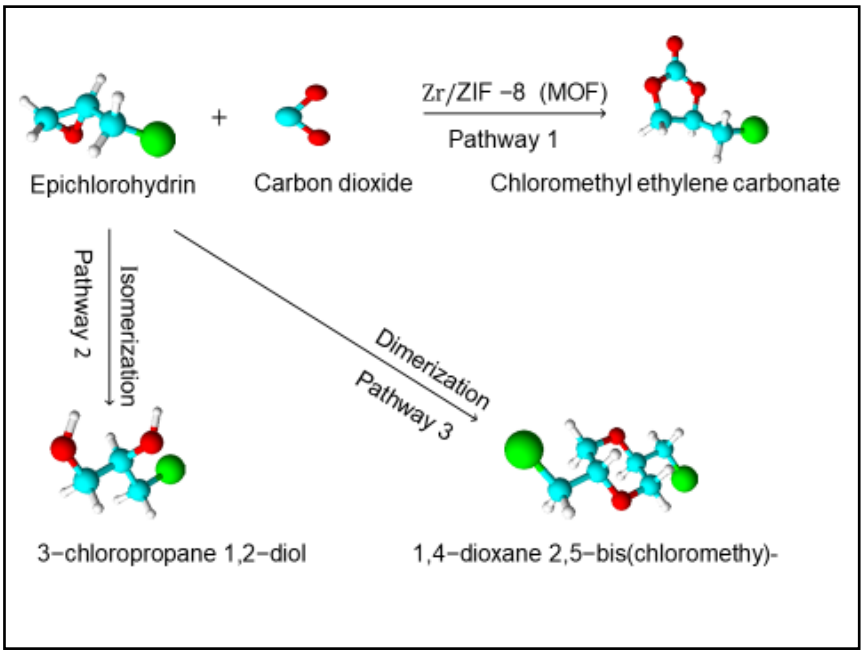

Figure 1. Reaction pathways for cycloaddition reaction of epichlorohydrin (ECH) and carbon dioxide (CO_2).

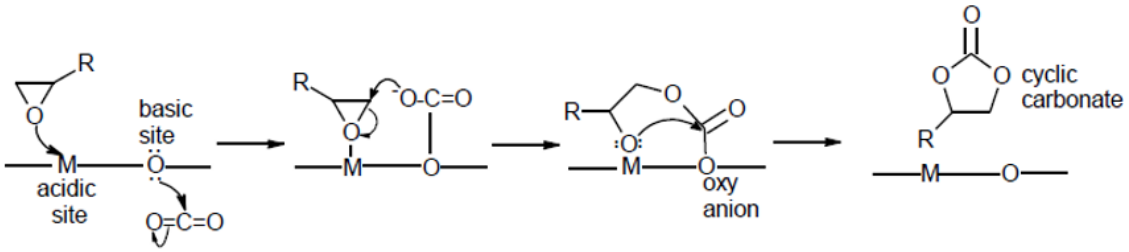

Figure 2. Proposed reaction mechanism for the cycloaddition reaction of CO_2 to ECH over an acid-base pairs. **R** is an alkyl group, **M** is a metal atom (acidic site), and **O** is oxygen atom (basic site).

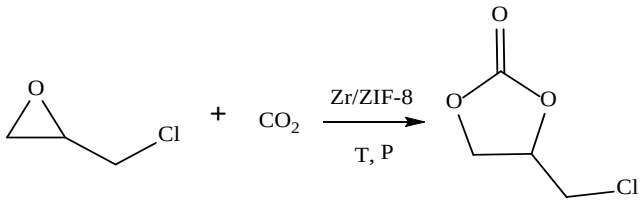

epichlorohydrin chloromethyl ethylene carbonate

Figure 3. Schematic representation of ECH–CO_2 cycloaddition reaction.

2.6. Catalyst Characterization

The powder X-ray diffraction (XRD) patterns of the samples was analyzed at room temperature with a characteristics peaks range of $5 < 2\theta < 35$ at a scanning rate of 0.5° min^{-1}. The catalyst was placed on a zero-background silicon sample holder using a Bruker D8 advance X-ray diffractometer in transmission geometry with CuKα radiation (λ = 1.5406° A) at 40 kV and 40 mA. The samples were slightly grinded before measurements were taken so as to prevent preferential orientation of individual crystals during sample analysis.

The Brunauer–Emmett–Teller (BET) surface area of the as-prepared catalyst was analyzed with a Micromeritics Gemini VII analyzer at room temperature (291 K). Prior to BET analysis, the samples were degreased in a turbomolecular pump vacuum at 423 K for 8 h. The surface area and nitrogen adsorption/desorption isotherm measurements were taken at liquid nitrogen temperature of 77 K (purge gas supplied by BOC, UK). In order to achieve greater degree of accuracy in the accumulation of the adsorption data, the Micromeritics Gemini analyzer was fitted with pressure transducers to cover the range of 133 Pa, 1.33 kPa, and 133 kPa.

The Fourier transform infrared (FTIR) spectra (4500–600 cm^{-1}) of the samples were obtained using Nicolet Magna-IR 830 spectrometer in KBr disks at room temperature with a resolution of 2 cm^{-1}. The specimen was mixed KBr in ratio 1:300, the mixture was ground in an agate mortar to a very fine powder. The product was oven dried for 12 h at 373 K, 250 mg of the dry samples were used to make a pallet; the pallet was analyzed, and the spectra were recorded by 32 scans with 4 cm^{-1}.

Particle size morphologies and microstructures of the as-synthesized Zr/ZIF-8 catalyst was examined using the JEOL JSM-35C instrument operated at voltage 20 kV acceleration. Prior to imaging, the specimen was carbon-coated (5–10 nm) under a vacuum condition using Emitech K550X sputter coater, this was done to enhance material conductivity. The particle mean size of the specimen were calculated by taking a manual measurement of about 300 crystals in the SEM images using the field emission scanning electron microscope (FE-SEM). FE-SEM spectra produced were used to examine the particle size and morphology.

Transmission electron microscopy (TEM) images of the catalyst were examined using a high resolution TEM (HRTEM). A sample of the specimen was sonicated in ethanol for 15 min and was then placed by a dropwise onto a carbon film-supported copper grid. The as-prepared sample was allowed to dry at room temperature before inserting into a sample holder. X-ray photoelectron spectroscopy (XPS) of the samples was recorded on the krato axis ultra DLD photoelectron spectrometer, a surface

science instrument SSx-100 using a monochromatic Al KR X-ray source operating at 144 W. Raman spectroscopy measurements of the specimen were taken at room temperature with the Horiba Jobin Yvon LabRAM spectrometer equipped with an aHeNe laser operating at a wavelength of 633 nm (E_{ex} = 1.96 eV) and Coherent Innova 70 ion laser at a wavelength of 458 nm, 488 nm, and 514 nm.

3. Results and Discussion:

Catalyst Characterization

The X-ray diffraction patterns of ZIF-8, Zr/ZIF-8 and recycled Zr/ZIF-8 are shown in Figure 4. The diffraction peaks appeared at small 2θ angles with eight diffraction peaks at 7.31, 10.31, 12.71, 14.71, 16.41, 18.01, 24.61, and 26.71 which are indexed to the (011), (002), (112), (022), (013), (222), (233), and (134) planes, respectively. The XRD patterns of both Zr/ZIF-8 and recycled Zr/ZIF-8 catalysts are identical as shown in Figure 4, confirming that Zr/ZIF-8 has high crystal stability under the normal reaction conditions. These results are in agreement with simulated patterns reported in other literature [25–28]. The decrease in peak intensity of these diffractions was also observed at (2θ = 28–35°) indicating the effect of excess doping of Zr into the ZIF-8 framework. The XRD pattern of Zr/ZIF-8 also show a characteristic peak of ZIF-8 with no diffraction peak of zirconium nitrate.

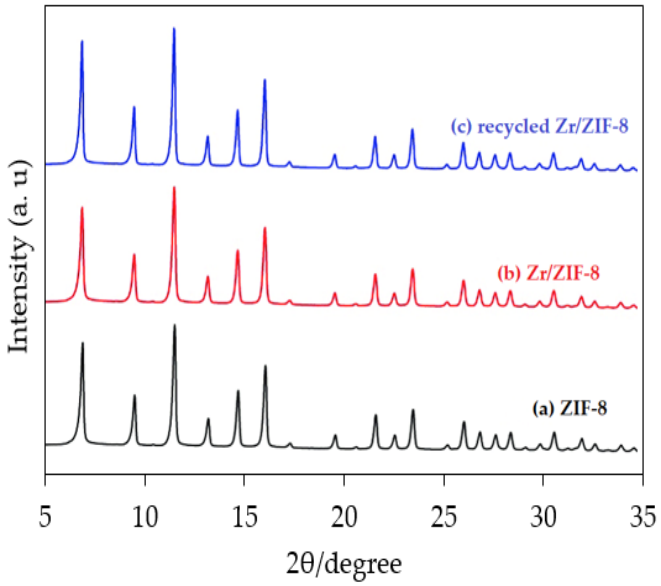

Figure 4. X-ray diffraction (XRD) patterns of (**a**) ZIF-8, (**b**) Zr/ZIF-8, and (**c**) recycled Zr/ZIF-8 catalysts.

Although, the peak intensity of Zr/ZIF-8 may be slightly lower when compared to commercial Basolite Z1200, purchased from Sigma Aldrich. Nevertheless, the experiments of Nordin et al. [29] They establishes that guest molecules (such as zirconium) occupying MOF pore spaces may cause pattern destructive and subsequently, a retarded gas uptake capacity in the MOF. A further and in-depth examination of the XRD patterns of the specimen beyond this study could reveal some surprising details as doping of zirconium into ZIF-8 could enlarge its pore spaces [30], thereby inducing a crystallographic defect in the Zr/ZIF-8 catalyst.

The nitrogen adsorption–desorption isotherms of ZIF-8, Zr/ZIF-8, and the recycled Zr/ZIF-8 catalysts are shown in Figure 5. The samples were measured at liquid temperature of 77k at 373 K for 24 h. The three isotherms showed an attribute of a microporous framework with a sharp hysteresis loop of P/P0 between 0.8 and 1.0. However, the pristine ZIF-8 catalyst demonstrates a typical type-I isotherm behavior [31] while Zr/ZIF-8 and the recycled Zr/ZIF-8 catalysts both shows typical type-IV isotherms with a type H_4 hysteresis loop in the range of P/P0 = 0.4–0.8 indicating the presence of mesopores [32]. Meanwhile, an increase in the volume adsorbed at low relative pressure is consistent with interparticle

voids, which is indicative of dual macro-mesoporosity of the Zr/ZIF-8 lattice according to International Union of Pure and Applied Chemistry (IUPAC) classification [33,34].

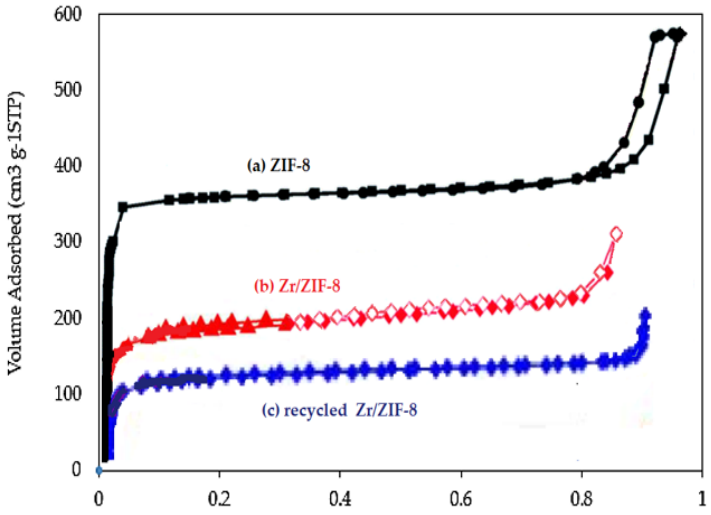

Figure 5. N_2 adsorption–desorption isotherms of (**a**) ZIF-8, (**b**) Zr/ZIF-8, and (**c**) recycled Zr/ZIF-8 synthesized with 10% dopant of Zr.

The specific BET surface area (S_{BET}) of the catalysts has been calculated using the BET equation. The pore size distribution was derived from the nonlinear density functional theory (DFT) model (calculated using computer software). The surface area and micropore volume of Zr/ZIF-8 was generally lower than ZIF-8 as shown in Table 1. The lower BET surface area and pore volume of Zr/ZIF-8 may be caused by the blockage of the pore cavities of the host molecule as a result of deposition of zirconium particles in the ZIF-8 shell, a phenomenon that has been previously reported by Na et al. [35]. Surprisingly, the total pore volume and the BET specific surface area of recycled Zr/ZIF-8 catalyst both decreased after the reaction. This observation may be attributed to agglomeration of coke deposits in the pore spaces, resulting in the blockage of some micropores and mesopores. [36].

Table 1. Comparison of Brunauer-Emmett-Teller (BET) surface area analysis, pore-volume, and pore size for ZIF-8 and Zr/ZIF-8 crystals.

Entry	Material	$S_{(BET)}$ ($m^2 \cdot g^{-1}$)	Pore Volume ($cm^3 \cdot g^{-1}$)	Pore Size (nm)
1	ZIF-8	1700	0.664	1.30
2	Zr/ZIF-8	1458	0.536	1.23
3	Zr/ZIF-8 (recycled)	1378	0.498	1.21

These results reflect a good pore size distribution of the samples microporous network [37,38]. Although, variation may exist in particles BET surface area and pore volume from one literature to another, this may be attributed to post-synthesis work-up procedures such as further purification processes and activation of MOF samples [39]. The BET surface area as shown in Figure 5 is in agreement with the previous literature [40].

Figure 6 shows the morphologies and microstructures of ZIF-8, fresh and recycled Zr/ZIF-8 catalysts using the scanning electron microscope (SEM) with an average particle size diameter of 100 µm. Figure 6a shows an evolution of ZIF-8 crystal from cubes with 6 faces (100) to intermediates shapes, and finally to a more stable equilibrium rhombic dodecahedral shape with edges exposing 12 faces (110) [41]. Figure 6b (Zr/ZIF-8) revealed very slight morphological alterations to the Figure 6a (ZIF-8) framework. The slight alterations are a genuine indication of a stable Zr/ZIF-8 catalyst comparing to the report of Pang et al. [41]. Furthermore, the hexagonal shape of the recycled catalyst in

Figure 6c showed a very small change after the cycloaddition reaction. A close examination of the SEM images of Figure 6a,b shows no significant effect of attrition on the overall particle aggregation between the two structures. The SEM image of recycled Zr/ZIF-8 in Figure 6c showed rather small isolated monodispersed particles with a well-defined truncated rhombic dodecahedron structure caused by the presence of dopant in the host molecule. Essentially, the SEM images of the samples are consistent with the XRD results and the thermal stability of Zr/ZIF-8 as shown in the catalyst reusability studies. It is worth mentioning that, the increased average crystal size of the recycled Zr/ZIF-8 catalyst in the range of ~100–170 nm (Figure 6c) may be attributed to Ostwald ripening and/or recrystallization effect [42], a phenomenon which explains a possible increase in the average crystal size of the reused catalyst during cycloaddition reaction, especially at a higher temperature (reaction temperature 353 K).

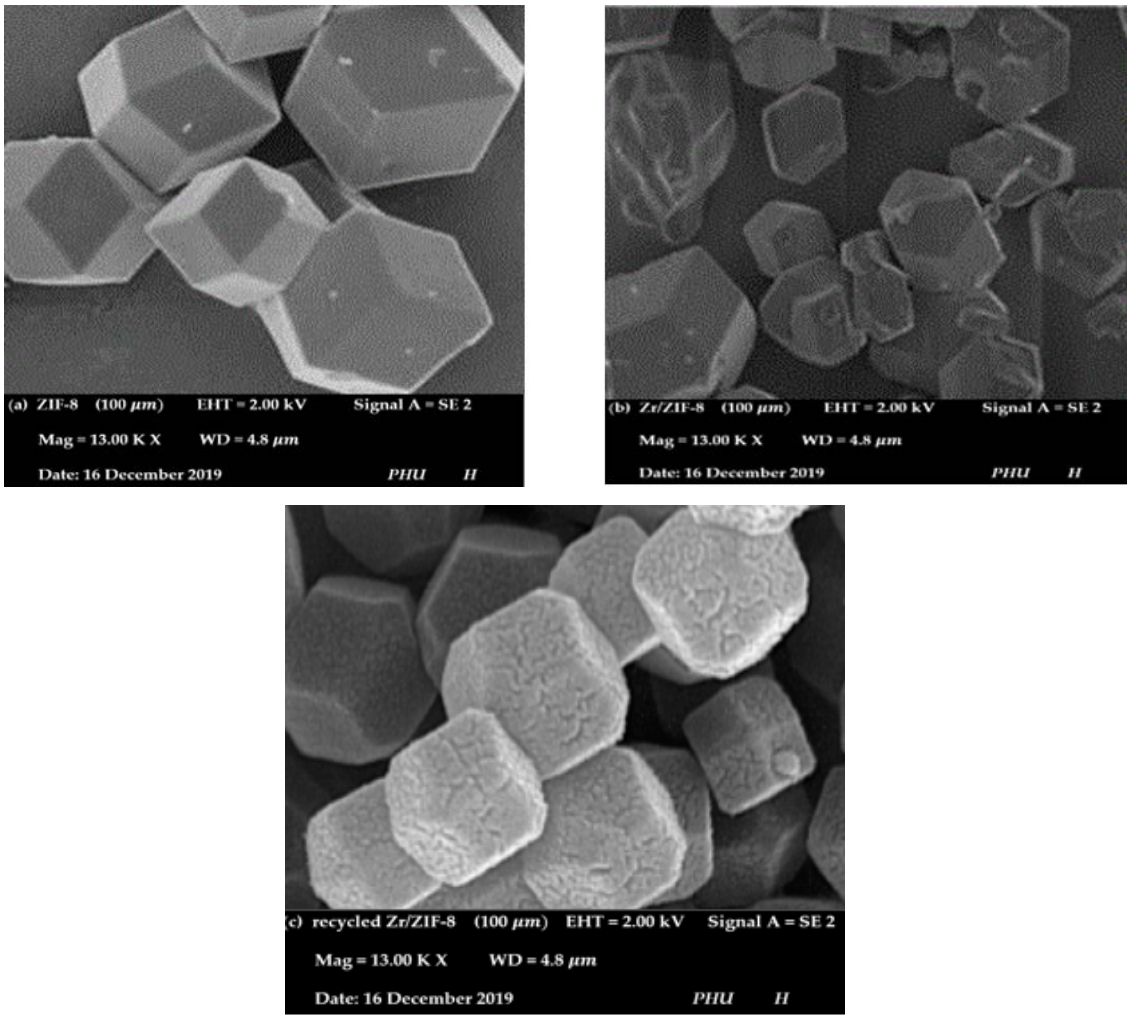

Figure 6. Scanning Electron Microscope (SEM) images of (**a**) ZIF-8 crystals, (**b**) Zr/ZIF-8, and (**c**) recycled Zr/ZIF-8 crystals synthesized with 10% dopant of Zr.

Low-magnification TEM images of the samples were carried out in order to examine the structural changes taking place on the surface of the samples. Figure 7a,b showed well-shaped high-quality homogenous crystals with a remarkable rhombic dodecahedral shape and average crystal size of about 100 μm which conforms to earlier literature [42]. It can be observed from the image in Figure 7b that there are no obvious aggregations or changes in particle size and morphology from Figure 7a. The TEM image of the recycled catalyst (Figure 7c) shows that the catalyst crystals were highly stable during the cycloaddition reaction of CO_2 and ECH.

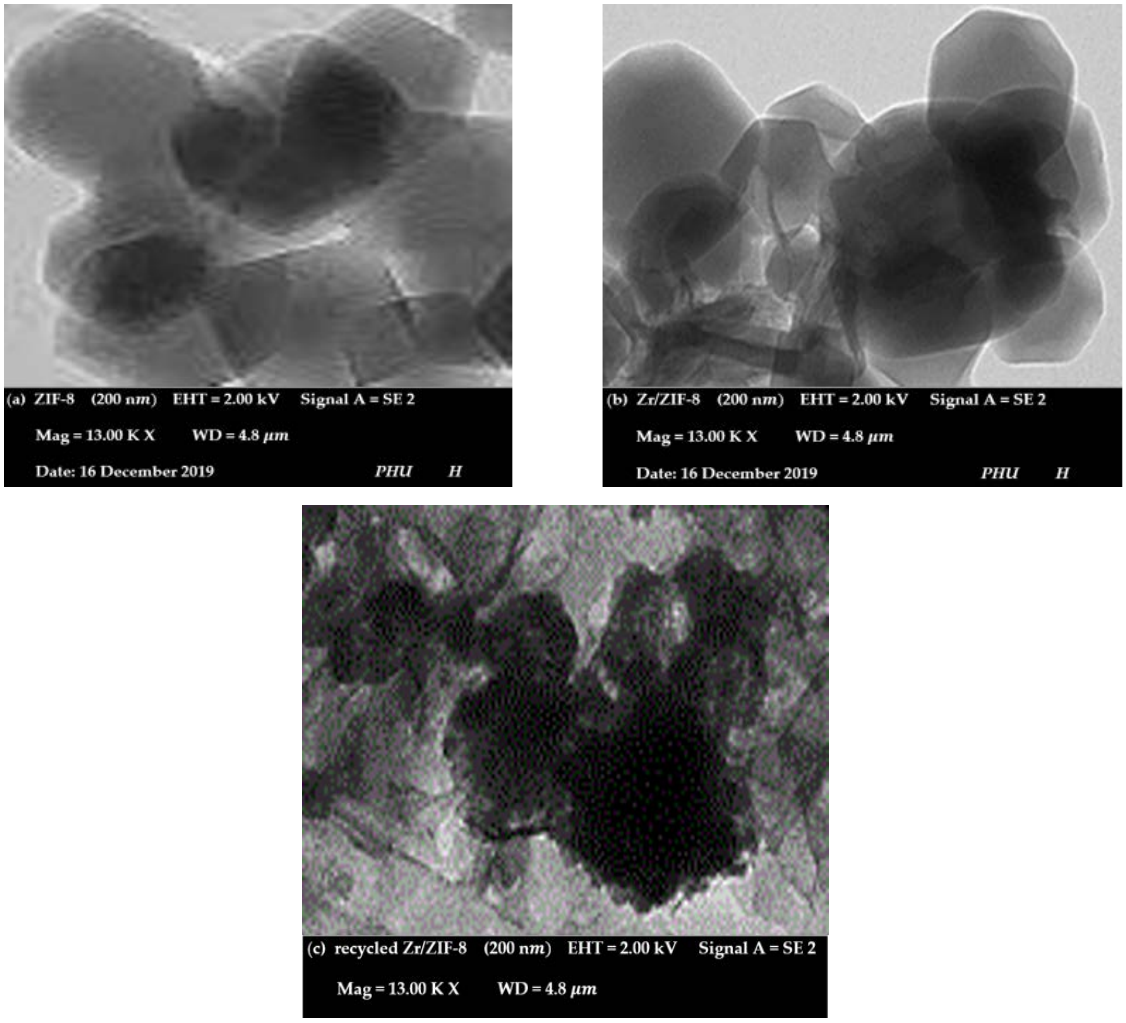

Figure 7. Transmission electron microscopy (TEM) image of (**a**) pristine ZIF-8 crystals, (**b**) Zr/ZIF-8, and (**c**) recycled Zr/ZIF-8 synthesized with 10% dopant of Zr.

Figure 8 shows the Fourier-transform infrared spectroscopy (FTIR) spectra of ZIF-8, Zr/ZIF-8, and the recycled Zr/ZIF-8 with an absorption region of 500–4000 cm^{-1}. The three samples show several bands with no substantial difference in the spectra. For example, a typical adsorption band at 423 cm^{-1} is attributed to the Zn–N bond vibrations indicating that zinc molecules of the imidazole ring are well-knitted during the reaction to nitrogen atoms in 2-methylimidazolate (2-Hmim) linkers to form the ZIF frameworks [43]. The absorption spectra at 2926 cm^{-1} can be ascribed to the aromatic moieties, while the spectra at 3133 cm^{-1} can be attributed to the aliphatic imidazole ring due to C–H stretching [44]. The missing adsorption spectra in the region of 3400 to 2200 cm^{-1} is a strong indication of a fully deprotonated imidazole ring during the formation of the ZIF-8 frameworks [44]. The strong sharp peak at 1449 cm^{-1} can be assigned to the C–C bonding in the benzene ring. The peak at 1579 cm^{-1} can be attributed to C=N vibrations mode [45], while the spectra in the band range between 1100 and 400 cm^{-1} can be assigned to C–N stretching vibrations. The small peaks at 1245 and 1255 can be assigned to C–N and C≡N groups respectively indicating the presence of imidazole molecules in the samples frameworks. The Zr–N bonding vibration located between 550 and 620 cm^{-1} in Zr/ZIF-8 catalyst [46]. All characteristic peaks of ZIF-8 can be observed both in Zr/ZIF-8 and the recycled Zr/ZIF-8, indicating a successful combination and interaction between Zr and ZIF-8. This observation is a strong indication that the frameworks of ZIF-8 have not been affected after the incorporation of Zr. This results in agreement with the report of Giraldo et al. [47] experiments.

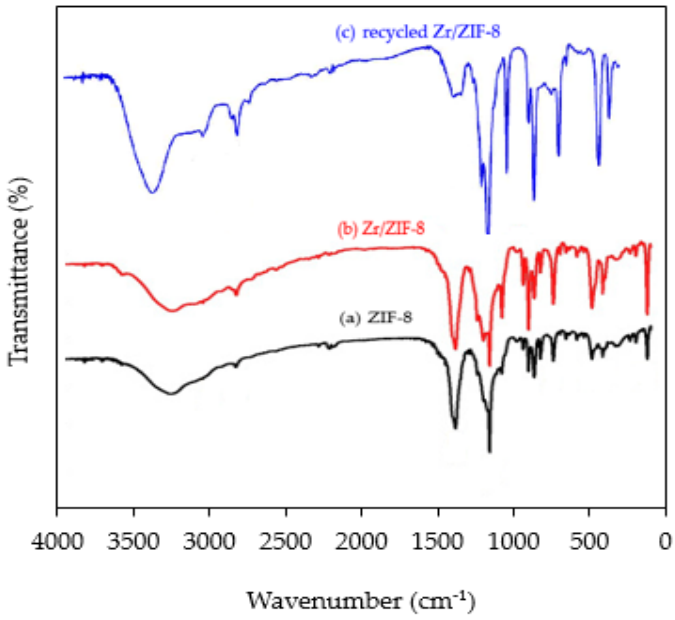

Figure 8. Fourier-transform infrared spectroscopy (FTIR) spectra of (**a**) ZIF-8, (**b**) Zr/ZIF-8, and (**c**) recycled Zr/ZIF-8 particles.

The X-ray photoelectron spectroscopy (XPS) spectra in Figure 9 clearly shows the chemical state of the element present in pristine ZIF-8 frameworks (Zn, C, N) and O, while those elements present in Zr/ZIF-8 sample include Zn, C, N, O, and Zr species. Figure 9a exhibits high resolution XPS spectra showing two strong peaks with binding energy of 1044.3 and 1021.1 eV which can be assigned to Zn $2p^{\frac{1}{2}}$ and Zn $2p^{3/2}$ components, respectively, confirming the presence of Zn (II) ions attached with nitrogen in the imidazole ring [48]. This result is consistent with the XRD results. With the incorporation of Zr into ZIF-8, the binding energy of Zn $2p^{1/2}$ and $2p^{3/2}$ have slightly increased, this could be as a result of the chemical environment of zinc and the interaction between zinc and zirconium. All spectra have been normalized to the magnitude of the Zn $2p^{3/2}$ and Zn $2p^{1/2}$ peaks, so that changes in intensity are relative to the amount of Zn in the surface region. Similarly, Figure 9b shows high-resolution N1s spectra of all samples. The N1s spectra can be deconvoluted into three characteristic peaks found at 399.0 and 399.8 and 398 eV which can be assigned to the pyridinic, pyrrolic, and graphitic, respectively. These can be related to the N species of the 2-methyl imidazole ring [48]. C1s spectra shows four different characteristic peaks corresponding to C–C at 284.1 eV, C–N at 285.8 eV, C–O at 286.4 eV, all assigned to the 2-methyl imidazole ring [48]. The low peak found at 283.4 eV could be as a result of Zr doping into ZIF-8 frameworks [48]. Figure 9d shows high resolution O1 spectra that has been deconvoluted into two characteristic peaks with binding energy 532.3 and 531.8 eV corresponding to O^{2-} found in Zn–O bonding and carboxylate species, respectively [49]. The relatively low peak intensity of Zr–O in O1s, C1s, and N1s is a strong indication that the ZIF-8 frameworks are not affected by the presence of dopant, which perfectly agreed with the result of Mao et al. [50].

Raman spectra of ZIF-8, Zr/ZIF-8 and the recycled Zr/ZIF-8 were observed using a Renishaw Ramascope 1000 (model: 52699). Figure 10 shows that Zr/ZIF-8 exhibited several Raman spectra at the following peaks 687, 892, 1149, 1186, 1462, 1568, 2931, 3114, and 3131 cm^{-1} similar to ZIF-8 spectra. The spectra at 1116 and 1484 cm^{-1} corresponding to bands D and G, respectively, found in the Raman spectrum of ZIF-8, have not been observed in the Zr/ZIF-8 and the recycled Zr/ZIF-8 spectra. This may be as a result of a split of the main bands at 1143 and 1508 cm^{-1} as previously reported by Biswal et al. [51]. The spectra found at 278 cm^{-1} may be attributed to Zn–N stretching, while the spectra at 683, 1143, 1456, and 1508 cm^{-1} are attributed to imidazole ring puckering, C5–N vibrations, methyl bending, and C4=C5 stretching, respectively, which are similar to the observation of Tanaka et al. [52]. The remaining spectra can be assigned to stretching and bending on the imidazole ring [53]. With

doping of Zr into the ZIF-8 frameworks, the peaks at 1116 and 1484 disappeared with no significant change in main peaks on spectra [54]. The spectra of three samples shows similar vibration modes, which confirms structural equality in the frameworks.

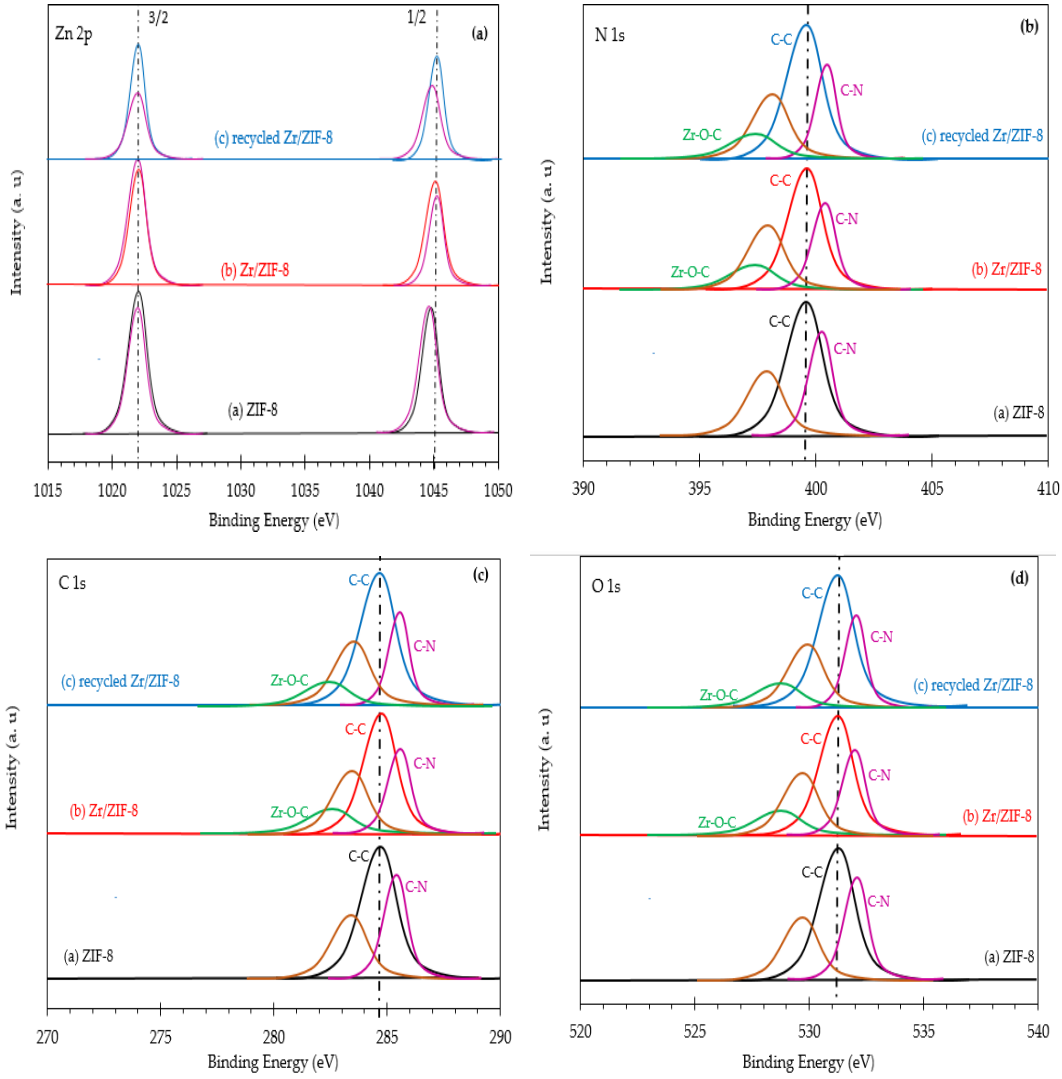

Figure 9. X-ray photoelectron spectroscopy (XPS) spectra showing deconvoluted regions of ZIF-8, Zr/ZIF-8 catalyst, and recycled Zr/ZIF-8 catalysts. (**a**) Zn 2p, (**b**) N 1s, (**c**) C 1s, (**d**) O 1s.

There are three distinct phases of weight loss experienced by both samples as indicated in Figure 11. It can be observed from the thermogram that, both catalysts experienced a very small initial weight loss of about 3% in the region from 298 to 373 K in the first phase. This can be attributed to loss of water and some guest molecules (e.g., methanol) and possibly some unreacted species trapped in the pore cavities of the framework. As the temperature was further increased through the second phase, Zr/ZIF-8 experienced a gradual and steady weight loss up to 723 K and then remained stable thereafter until 973 K. Conversely, ZIF-8 experienced a rapid and significant weight loss of around 54% up to 823 K, attributing the decomposition of some absorbed organic ligand and the final weight loss phase experienced the collapse of the ZIF-8 structure at high temperature [53]. It is worth noting that materials stability of the ZIF-8 framework can be attributed to the incorporation of zirconium in ZIF-8. A similar observation was reported by Wang et al. [54] in the doping of lanthanum into ZIF-8. After the decomposition, approximately 39% of the starting weight remained. From this observation,

it can be concluded that the Zr/ZIF-8 catalyst frameworks have remained structurally stable and this is consistent with XRD and SEM.

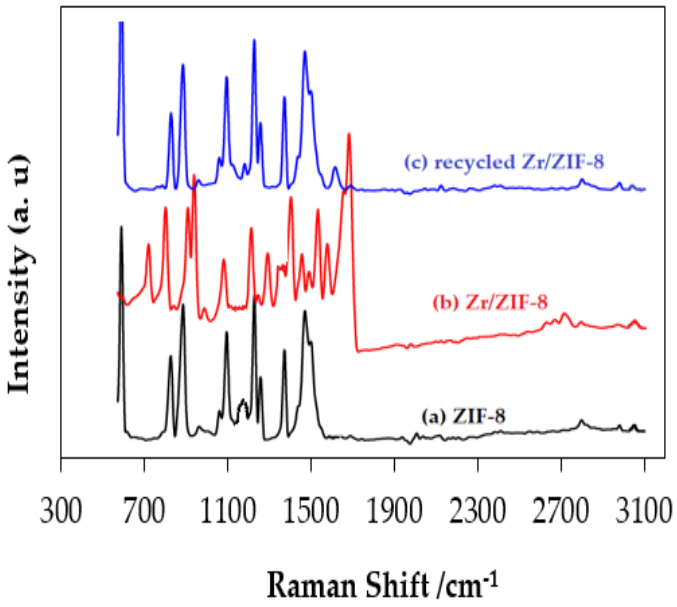

Figure 10. Raman spectra of the crystal-size (**a**) ZIF-8, (**b**) Zr/ZIF-8, and (**c**) recycled Zr/ZIF-8 samples.

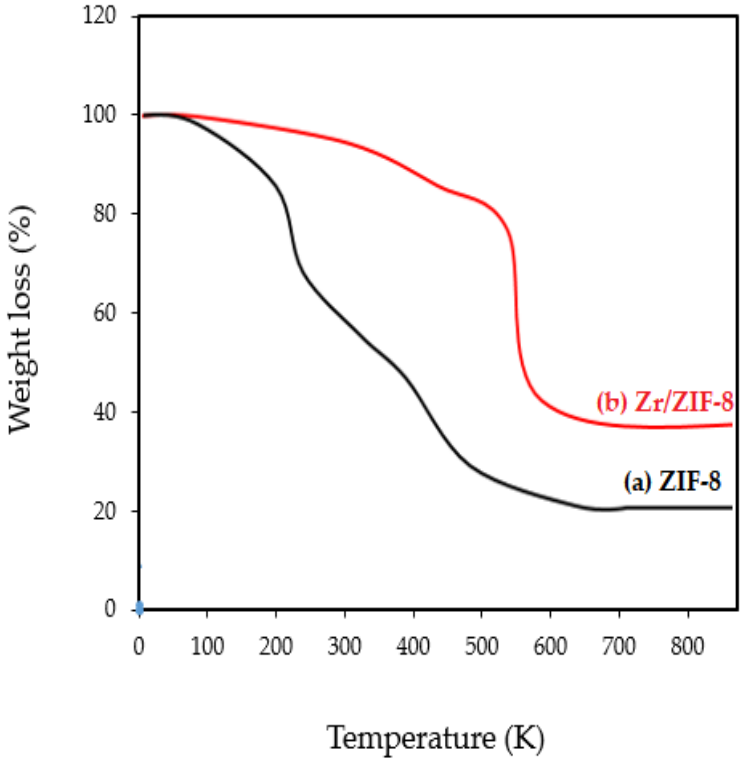

Figure 11. Thermal stability curve of (**a**) ZIF-8 and (**b**) Zr/ZIF-8.

4. Catalytic Activity

After catalyst characterization, the catalytic activity of the novel materials was compared with ZIF-8 for the synthesis of chloromethyl ethylene carbonate from CO_2 and epichlorohydrin under solvent-free conditions. It is interesting to note that the combination of acid and basic sites (Lewis and Brönsted site) existing in the MOF catalyst may improve the catalytic activity of both samples.

The reactions were carried out under the same conditions of 353 K reaction temperature, 8 bar CO_2 pressure, 10% (*w/w*) catalyst loading, 8 h reaction time, and 350 rpm of stirring speed.

From the Table 2, it follows that at optimum CO_2 pressure of 8 bar, reaction time of 8 h, catalyst loading of 10 % *w/w*, and variable temperature, Zr/ZIF-8 exhibits a higher catalytic activity than ZIF-8 (Zr/ZIF-8: 93%, 86%, 76%; and ZIF-8: 77%, 74%, 52%) for conversion, selectivity, and yield respectively at the same reaction conditions. The presence of acid and/or basic site in heterogeneous catalyst has significantly catalyzed the reaction of CO_2 and ECH to produce CMEC [42].

Table 2. Summary of catalytic performance of ZIF-8 and Zr/ZIF-8 for coupling reaction of CO_2 and epichlorohydrin to produce chloromethyl ethylene carbonate.

Entry	Catalyst	T (K)	Conversion (%)	Selectivity (%)	Yield (%)
1	ZIF-8	323	65	57	37
2	ZIF-8	333	69	64	44
3	ZIF-8	343	73	69	49
4	ZIF-8	353	77	74	52
5	ZIF-8	363	81	71	51
6	ZIF-8	373	85	69	49
7	Zr/ZIF-8	323	80	67	58
8	Zr/ZIF-8	333	86	74	64
9	Zr/ZIF-8	343	90	80	70
10	Zr/ZIF-8	353	93	86	76
11	Zr/ZIF-8	363	95	85	75
12	Zr/ZIF-8	373	97	82	72

4.1. Effect of Different Heterogeneous Catalysts

Catalysts are very important parts of any chemical reaction; they contain active sites, which are able to speed up the kinetics of chemical reaction by reducing the activation energy. Different types of homogenous and heterogeneous catalysts have been synthesized to catalyze the reaction of CO_2 and epoxide to produce corresponding organic carbonates. In order to assess the stability and effectiveness of the samples, the catalytic activity of both ZIF-8 and Zr/ZIF-8 was investigated in the synthesis of chloromethyl ethylene carbonate from CO_2 and epichlorohydrin. Table 2 shows the effects of the two catalysts for the conversion of epichlorohydrin, selectivity and yield of chloromethyl ethylene carbonate. The catalysts were synthesized using solvothermal method as per standard procedures. The samples were heat-treated at about 373 K in order to enhance an improved catalytic activity and were labelled as ZIF-8 and Zr/ZIF-8 for pure and doped samples, respectively. The reaction of CO_2 and ECH to produce CMEC was carried out in a 25 mL high-pressure reactor at 353 K reaction temperature, 8 bar CO_2 pressure, 10% catalyst loading, and 8 h reaction time. It can be seen from Table 2 that when ZIF-8 was used to catalyze the reaction of CO_2 and ECH, the conversion of ECH, selectivity, and the yield of CMEC were 77%, 74%, and 52% respectively. However, incorporating zirconium into ZIF-8 has significantly increased catalytic performance of Zr/ZIF-8 with the conversion of ECH, selectivity and the yield of CMEC being 93%, 86%, and 76% respectively, although, the presence of side products were reported in both reactions by GC analysis. These side products include 3-chloropropane 1,2-diol and 2,5-bis (chloromethyl)-1,4-dioxane.

With similar pore spaces and same embedded Lewis acid metal sites in both ZIF-8 and Zr/ZIF-8 catalysts, the increase in the catalytic activity of Zr/ZIF-8 as shown in Figure 12, may be ascribed to high CO_2 affinity via the introduction of zirconium into MOF, which has significantly increased those pore spaces of ZIF-8 [55]. A fine balance of proximity between pure and Zr-doped MOF was critically examined by Demir and research group. Their experimental results in the solvent-free coupling reaction of ECH and CO_2 to produce epichlorohydrin carbonate (ECHC) concluded that 79.6% yield of ECHC and 97.3% selectivity were achieved after 2 h using Zr-MOF catalyst (Zr/MOF-53). It is however

interesting to note that GC analysis of the product of Zr/ZIF-8 identified 3-chloropropane-1,2-diol (diols of epichlorohydrin-14.2%) as the main reaction by-products.

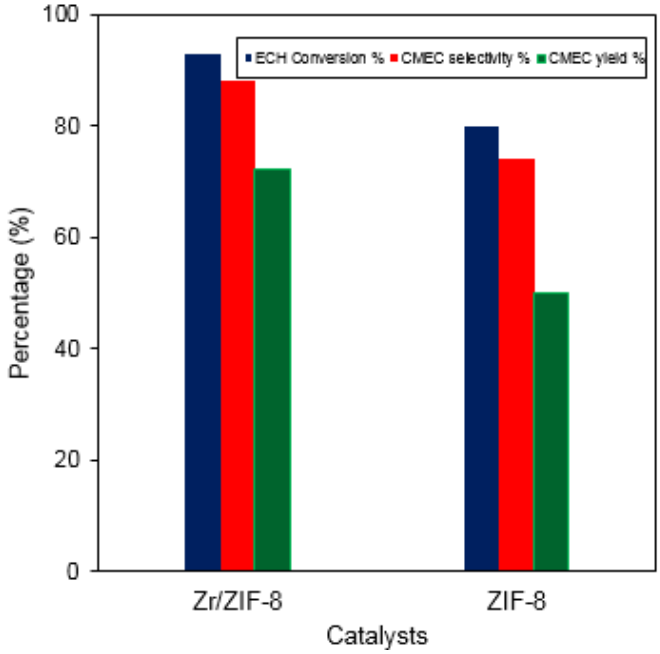

Figure 12. Effect of different catalysts on the cycloaddition reaction of epichlorohydrin (ECH) and carbon dioxide (CO_2) to produce chloromethyl ethylene carbonate (CMEC) with reaction conditions of 353 K reaction temperature, 8 bar CO_2 pressure, 10% catalyst loading, 8 h reaction time, and 350 rpm of stirring speed.

To affirm the superior catalytic performance of Zr/ZIF-8 over ZIF-8, nitrogen adsorption and desorption isotherms of the two frameworks were collected and presented in Table 1. Zr/ZIF-8 showed higher CO_2 adsorption capacity which explains in part the improved catalytic performance.

4.2. Effect of Temperature

The cycloaddition reaction of CO_2 and epoxide can be referred to as exothermic in nature. The influence of temperature on the cycloaddition of CO_2 to ECH to produce CMEC was investigated between temperature ranges of 323 to 373 K. All experiments were conducted with optimized reaction conditions, which were determined during our previous studies with a 10% catalyst loading and 8 bar CO_2 pressure for 8 h and a stirring speed of 350 rpm. Table 2 shows the catalytic performance of Zr/ZIF-8 and ZIF-8 as a function of temperature, CO_2 pressure, reaction time, and catalyst loading. It can be depicted from Figure 13 that the conversion of epichlorohydrin, selectivity and yield of CMEC were temperature-dependent. Generally speaking, variation in temperature has similar trends in the catalytic activity of both frameworks; the conversion of epichlorohydrin, the selectivity and yield of CMEC increases as temperature increases from 323 to 353 K. However, incorporating zirconium into ZIF-8 has significantly improved the performance of Zr/ZIF-8 with the conversion of ECH, selectivity and yield of CMEC as 93%, 86%, and 76% respectively, while ZIF-8 gave a conversion of ECH, selectivity and yield of CMEC as 77%, 74%, and 52%, respectively, under the same optimum reaction temperature.

Further increase in reaction temperature beyond 353 K was unfavorable to selectivity and yield of CMEC in both systems. A slight decrease of the CMEC yield (from 76% to 75%; Zr/ZIF-8 and 52% to 51%; ZIF-8) was observed upon an increase in temperature. This may be due to the formation of diols and dimers of epichlorohydrin [56] and a small amount of by-products such as polymerized CMEC could also affect the yield. Adeleye et al. [57] reported that the increase in the reaction temperature caused a decrease in carbonate yield, due to the decomposition of the catalyst at a higher temperature.

Kim et al. [58] also concluded that the reaction temperature for optimal performance is dependent on the nature of the catalyst employed. Therefore, for this set of experiments, the optimized reaction temperature for both frameworks in the synthesis of chloromethyl ethylene carbonate was 353 K. All the subsequent experiments for the chloromethyl ethylene carbonate were conducted at 353 K.

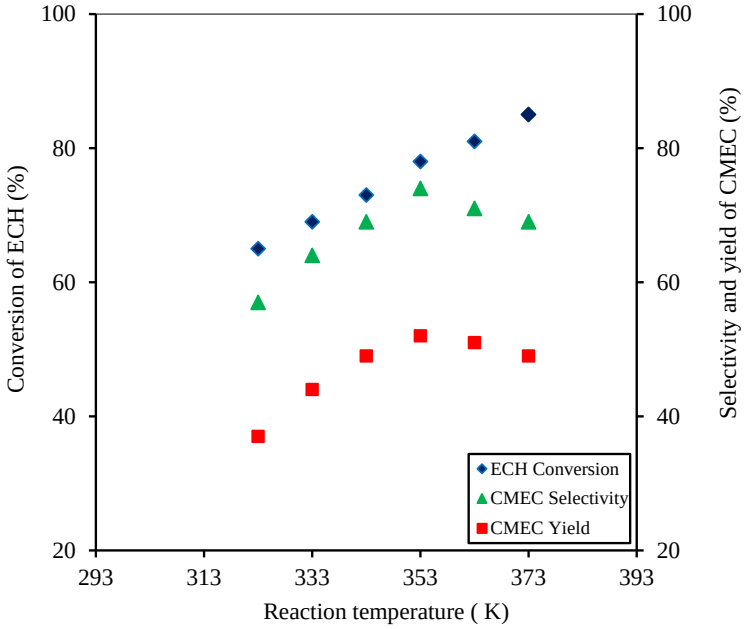

(**a**) **ZIF-8**

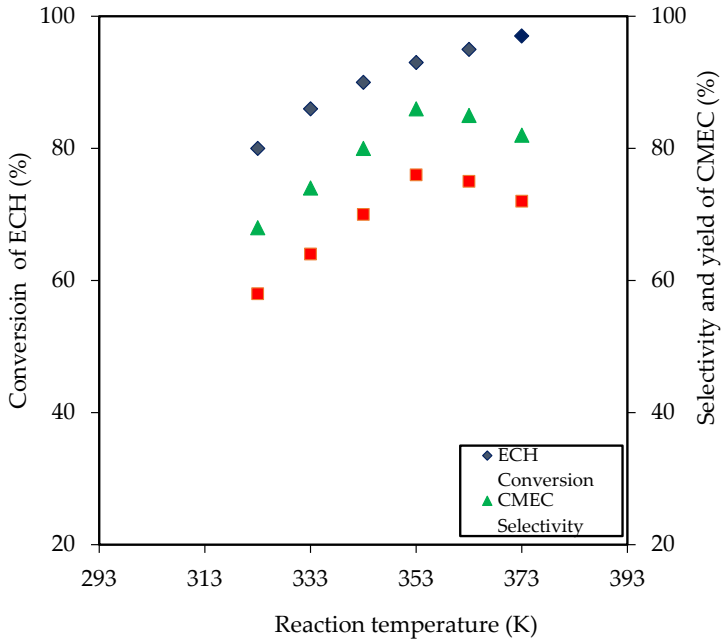

(**b**) **Zr/ZIF-8**

Figure 13. Temperature dependence on conversion of ECH versus selectivity and yield of CMEC. Experimental conditions: catalyst (**a**) ZIF-8 and (**b**) Zr/ZIF-8; catalyst loading 10% (*w*/*w*); reaction time 8 h; CO_2 pressure 8 bar; stirring speed 350 rpm.

4.3. Effect of CO_2 Pressure

CO_2 pressure is another important factor influencing the cycloaddition of CO_2 to epoxides. The pressure of carbon dioxide has been established as one of the most crucial factors affecting the conversion, yield, and selectivity of cyclic carbonate [59]. The reaction of epichlorohydrin and CO_2 to produce chloromethyl ethylene carbonate was examined by varying the CO_2 pressures. For this study, the experiments were carried out at 353 K, 10% catalyst loading, and 350 rpm for 8 h.

The selectivity and yield of CMEC was found to increase steadily from 67% and 58% to 86% and 76%, respectively, as the CO_2 pressure increases from 2 to 8 bar. These results indicate that the catalytic performance of the Zr/ZIF-8 depends on the concentration of available CO_2 at the reactive sites. Similar variation was observed in the catalytic activity of the two frameworks with changing CO_2 pressure where the selectivity and yield of CMEC increased from 57% and 37% to 77% and 52%, respectively, at the same pressure of 8 bar of CO_2 as in the case of Zr/ZIF-8.

Figure 14 demonstrates the dependence of CO_2 pressure on the yield of CMEC. It can be observed from the graph that the CMEC yield increased with increasing pressure, the maximum of the CMEC yield was reached at 8 bar. By increasing the CO_2 pressure more than 8 bar, a negative effect was observed on both reaction systems, where both yield and conversion experience a slight drop. Wang et al. [60] observed that the introduction of too much CO_2 dissolves in epoxide may result in the formation of CO_2-epoxide complex, and retards the interaction resulting in a lower conversion. Similar results were also reported by Onyenkeadi et al. [61], where the introduction of higher pressure of CO_2 dissolved in the epoxide and becomes an unfavorable factor due to the difficulty of separating CO_2 and ECH. This condition inhibits the reaction between ECH and catalyst, thus resulting in lower yield [62]. Liang et al. [63] also reported that many diols and dimers of epichlorohydrin were produced as side products at high pressure. Based on the experimental results and theoretical study, it can be concluded that 8 bar CO_2 pressure was the optimum and all subsequent experiments for the CMEC synthesis were carried out at a CO_2 pressure of 8 bar.

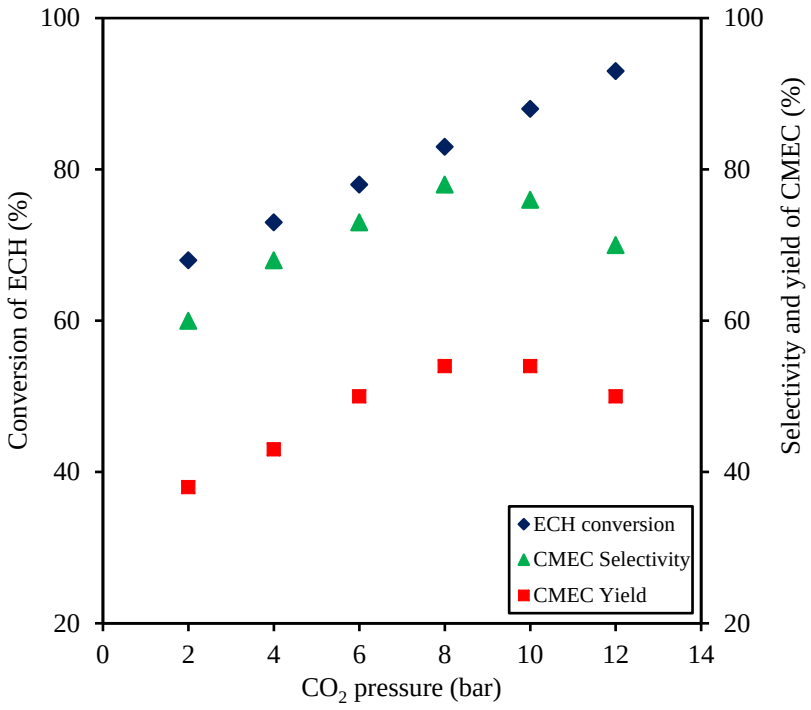

(a) ZIF-8

Figure 14. *Cont.*

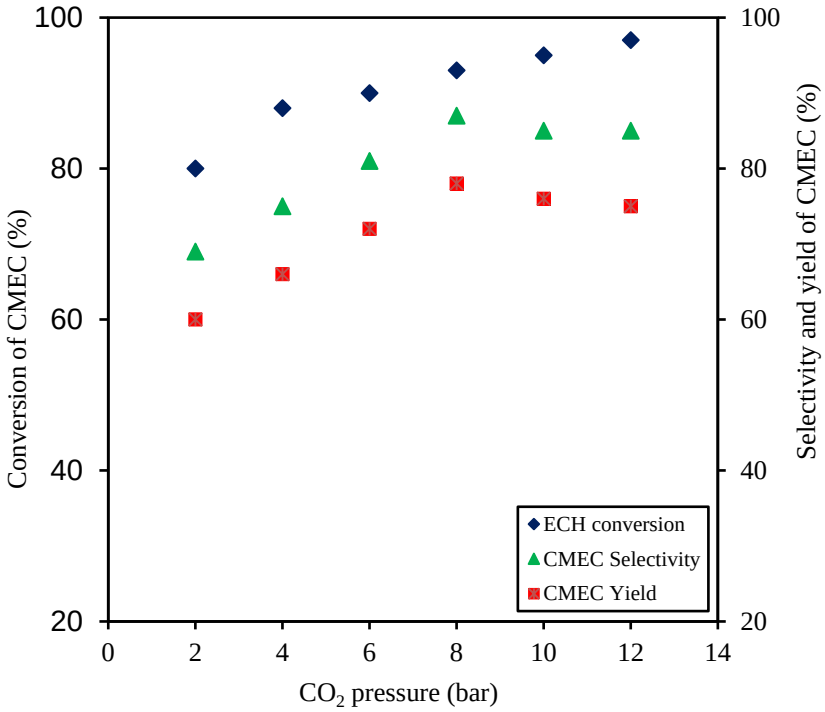

(**b**) **Zr/ZIF-8**

Figure 14. Pressure dependence on conversion of ECH versus selectivity and yield of CMEC. Experimental conditions: catalyst (**a**) ZIF-8 and (**b**) Zr/ZIF-8; catalyst loading 10% (*w*/*w*); reaction time 8 h; reaction temperature 353 K; stirring speed 350 rpm.

4.4. Influence of Reaction Time

The effect of varying the reaction time on the yield of CMEC was investigated by carrying out a set of coupling reaction of CO_2 and epichlorohydrin using both ZIF-8 and Zr/ZIF-8 catalysts. For this study, all experiments were conducted at 353 K and 8 bar CO_2 pressure with 10% (*w*/*w*) catalyst loading of ZIF-8 and Zr/ZIF-8. Figure 15 demonstrates the influence of reaction time on CMEC yield and selectivity. The results shown on the graph illustrates that the yield increased continuously at the beginning and reached 76% and 52% within 8 h for Zr/ZIF-8 and ZIF-8, then decreased to 75% and 51% respectively, indicating that a slight change in the reaction condition can influence the product formation in a reaction. Similarly, the conversion of ECH was observed to increase from 353 to 366 K when the reaction time was increased from 2 to 8 h. However, when the reaction time was increased further to 10 h and above, a progressive decrease in conversion of ECH was recorded. A similar observation was previously reported in the conversion of ECH to chloropropene carbonate with Zn-ZIF-67 by Adeleye et al. [64]. According to him, conversion of epoxides reaches an equilibrium plateau at optimum reaction time. This phenomenon is referred to as induction period. The induction period is attained when the CO_2 and epoxides sufficiently diffuse into the catalytic frameworks of the ZIF-material to reach the active sites of the catalyst and then be converted to the organic carbonate. Beyond the induction period, low conversion of epoxides as well organic carbonates may be observed. From Figure 15, it can be concluded that prolonged reaction time produces lesser ECH conversion and consequently lesser CMEC yield and selectivity. Based on the experimental results and theoretical study, the reaction time of 8 h was considered the optimum for ZIF-8 and Zr/ZIF-8.

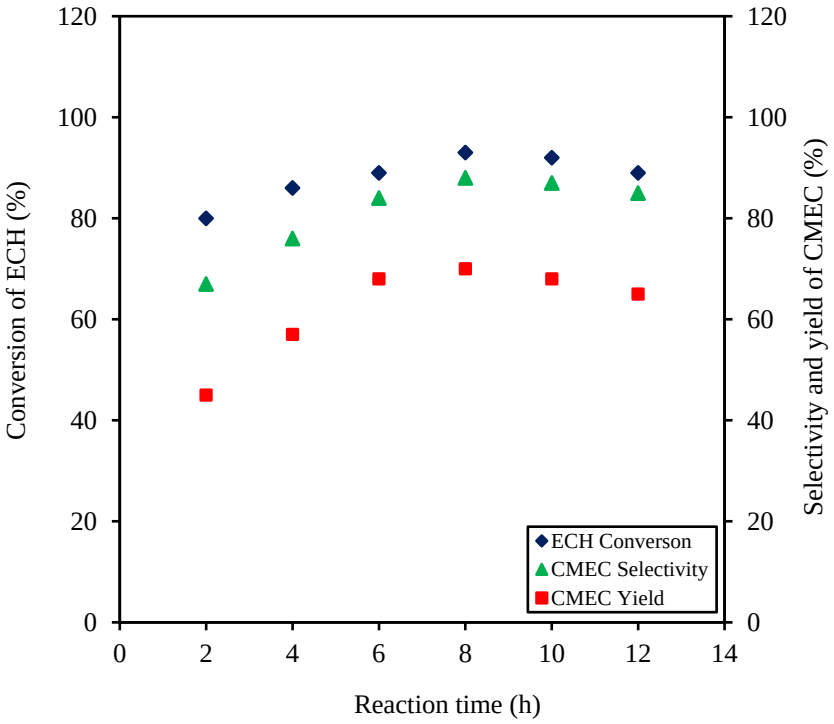

Figure 15. Time dependence on conversion of ECH versus selectivity and yield of CMEC. Experimental conditions: catalyst Zr/ZIF-8; catalyst loading 10% (*w/w*); reaction temperature 353 K; CO_2 pressure 8 bar; stirring speed 350 rpm.

4.5. Effect of External Mass Transfer in Heterogeneous Catalytic Processes

Mass transfer limitations play significant roles in chemical reactions by controlling the rate of reaction towards the desired product. In homogenous catalytic reaction, the effect of mass transfer between the phases is mostly negligible. However, in a heterogeneous catalytic reaction, the reaction rate significantly relies on the mass or diffusion between these phases. Mass transfer is typically higher in porous solid or fine particles of nanoscale than large nonporous catalyst [65], transfer of material from the exterior to the interior of a particle happens through pores that open to the external surface, which provides access to the interior of the crystallite material [65]. A typical example is zeolitic imidazolate framework (ZIF-8).

In the heterogeneous catalytic conversion of CO_2 and epoxide, the internal and external gradient of transport materials between system phases lowers the activity and selectivity of the catalyst towards the desired product [66]. It is important to know that when designing a new catalyst and directing such a catalyst to be selective towards a particular desired product mass transfer resistance and the kinetics are key functions [66]. In cycloaddition reaction of CO_2 with ECH, the physicochemical properties of the catalyst and the operating conditions all have a direct effect on the activity of the catalyst as well as the quality of CMEC formed [67]. When a chemical reaction occurs on an active surface, intraparticle diffusion takes place through the pores and the film surrounding the solid catalyst [67].

The coupling reaction of ECH with CO_2 to produce chloromethyl ethylene carbonate is an exothermic reaction. In order to reduce or eliminate the effects of mass transfer resistance, it is recommended to employ a highly porous heterogeneous catalyst [68]. The influence of mass transfer on the reaction of ECH and CO_2 to synthesize CMEC at 353 K reaction temperature for 8 h with a range of stirring speed between 320 and 550 rpm in an autoclave reactor. It was observed that there was no significant change in the conversion of ECH (~93), selectivity (~86), and the yield of CMEC (~76) when the stirrer speed was maintained above 330 rpm. Therefore, it was concluded that there was no effect of external mass transfer resistance on the experimental conditions.

4.6. Effect of Catalyst Loading

To investigate the influence of catalyst loading on the CMEC synthesis, several number of experiments were performed by varying the molar ratio of both ZIF-8 and Zr/ZIF-8 catalyst to ECH. For this study, all experiments were conducted at 353 K and 8 bar CO_2 pressure for 8 h. The results of varying catalyst loading are presented in Figure 16. It can be observed from the graph that by increasing the catalyst loading, there was a corresponding increase in ECH conversion, yield, and selectivity of CMEC. For example, for the experiments conducted with catalyst loadings from 2.5%–7.5%, there was a significant increase in ECH conversion, yield, and selectivity of CMEC. Also, for the experiment conducted at 10% (*w/w*) of catalyst loading, there was a sharp increase of ECH conversion, yield, and selectivity of CMEC from 90%–96%, 45%–56%, and 73%–79%, respectively. According to Maeda et al. [68], the decrease in epoxide conversion may be ascribed to a decrease in the substrate concentration around the pore cavities of the catalyst at higher catalyst loading. This effect neutralizes the Brönsted acid centers of the catalyst, thereby preventing the interaction between the acidic sites of the catalyst and the oxygen atom of epoxide from the ring opening. This consequently reduces the epoxides conversion to organic carbonates. Considering the percentage error of ±2%, it can be concluded that the number of active sites for ECH and CO_2 to react and produce CMEC was large enough at 10% (*w/w*) catalyst loading. From the results obtained with respect to catalyst loading, 10% (*w/w*) was the optimum. From the experimental results for both ZIF-8 and Zr/ZIF-8 catalysts, it is satisfactory to conclude that 10% (*w/w*) catalyst loading was considered the optimum and further experiments were carried out at 10% (*w/w*) catalyst loading.

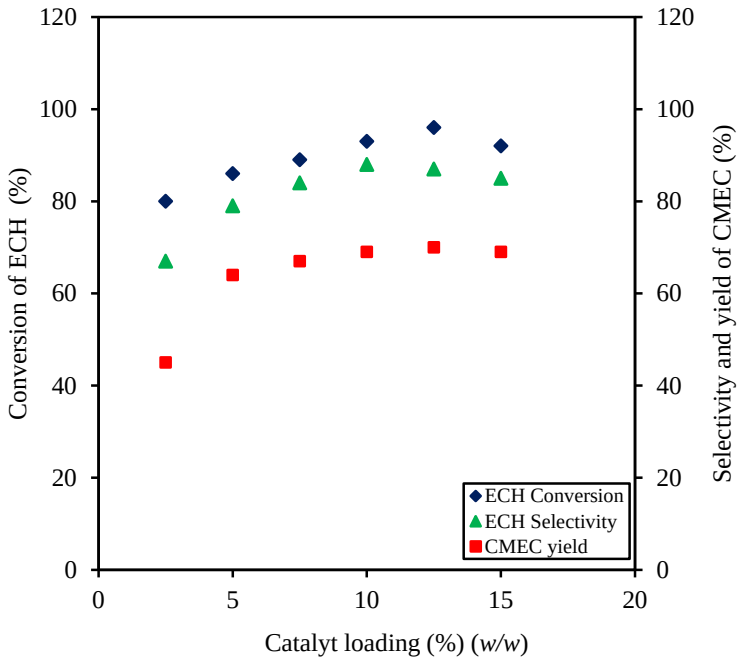

Figure 16. Catalyst loading dependence on conversion of ECH versus selectivity and yield of CMEC. Experimental conditions: catalyst Zr/ZIF-8; reaction temperature 353 K, (*w/w*); reaction time 8 h; CO_2 pressure 8 bar; stirring speed 350 rpm.

4.7. Effect of Reaction Conditions on Catalysts Selectivity to Chloromethyl Ethylene Carbonate

Figure 13a,b shows the effect of varying reaction temperature on catalysts' selectivities towards CMEC. For example, it can be observed that when the temperature was increased from 50 to 80 °C, both catalysts show a corresponding increase in selectivities from 68% and 50% to 86% and 74%, respectively. However, when the temperature was increased beyond the 353 K, a marginal decrease in selectivities was observed in both frameworks, demonstrating that the 353 K was the optimum temperature for the

reaction. Meanwhile, the gas chromatography–mass spectroscopy (GC-MS) analysis of the samples shows that 17.3% of 2,5-bis (chloromethyl)-1,4-dioxane (by-product) formed at 353 K, this may explain in part why a drop in catalysts' selectivities was recorded for both samples. Similar results and by-product have been previously reported with ZIF-8 by Carron et al. [69]. They also agree that almost 100% selectivity of ZIF-8 to chloropropene carbonate was achieved at a temperature of 393 K, but decreased to 78.6% when the temperature was increased to 403 K.

In addition to the effect of temperature on catalysts' selectivities, the influence of varying CO_2 pressure on catalysts' selectivities was also investigated. According to Figure 14a,b, the selectivity of the catalysts towards CMEC was found to increase steadily from 67% and 58% to 86% and 76%, respectively, as the CO_2 pressure was increased from 2 to 8 bar. These results indicates that the activity and selectivity of both catalysts were influenced by the concentration of available CO_2 at the reactive sites. Although, similar effect was observed in the responses of both catalysts to variation in CO_2 pressure, however, the results show that Zr/ZIF-8 has higher selectivity than the ZIF-8 catalyst, where the selectivity of both catalysts increased from 69% and 60% to 87% and 77%, respectively, for Zr/ZIF-8 and ZIF-8catalysts. Concersely, both samples experienced decline in selectivities from 87% and 77% to 85% and 70% for ZIF-8 and Zr/ZIF-8, respectively, when the CO_2 pressure was increased beyond the optimum level of 8 Bar.

Miralda et al. [70], further argues that ZIF-8 is a dual-functional catalyst with both acidic and basic sites that have been associated with the Lewis acid Zn^{2+} ions and the basic imidazole groups, respectively. This bifunctional characteristic enhances the catalyst selectivity for cycloaddition reaction. In a separate report, Miralda et al. [70], also ascertained that it is likely that Lewis acid sites associated with Zn^{2+} ions in the ZIF-8 framework play the vital role in catalyzing the reaction of epichlorohydrin and CO_2 to chloropropene carbonate. They further explained that the presence of basic nitrogen atoms of the imidazole ligand, probably, favours the adsorption and binding of CO_2 as well as activation of the carbon-oxygen bonds in CO_2**.** In agreement with other similar doped ZIF-8, the open metal centers in the Zr/ZIF-8 has the potential to easily activate the epoxides and the basic sites present in the frameworks. This could be the reason for the higher selectivity that were observed in the solvent-free ECH–CO_2 cycloaddition reactions under mild conditions. Comparatively, the higher selectivity of Zr/ZIF-8 than ZIF-8 towards CMEC may be attributed to the presence of zirconium (Zr). According to a 2019 publication by de Caro et al. [71], the effect of Zr doping on Mg-Al hydrotalcite, the catalyst has significantly increased its selectivity from 90% to >99% towards glycerol carbonate (GC).

4.8. Reusability of ZIF-8 Catalysts

Reusability is an important and essential feature of any heterogeneous catalyst in order to be considered useful in industrial applications [71]. The influence of catalyst reusability on the catalytic properties of ZIF-8 and Zr/ZIF-8 in the cycloaddition reaction was investigated. The experiments were carried out in a high-pressure reactor at optimum reaction conditions, i.e., at 353 K, 8 bar with fresh 10% (*w/w*) ZIF-8 catalyst loading, for 8 h, and at a stirring speed of 350 rpm. The catalysts after Run 1 in the cycloaddition reaction were washed with ethanol and acetone, centrifuged, and oven-dried at 343 K for 12 h before reuse. The recovered catalysts were reused for up to 7 subsequent experiments following the same experimental procedure. ZIF-8 showed a progressive loss in catalytic activity after each run as shown in Figure 17, while Zr/ZIF-8 exhibited no loss of activity indicating the catalyst stability for cycloaddition reaction of CO_2 epichlorohydrin. Yuan et al. [72] stated that the presence of dopant in ZIF-8 show that zirconium is more stable and resilient during the reaction. There was no significant change in the conversion of ECH, selectivity, and yield of CMEC using Zr/ZIF-8. Although, a very slight decrease in the yield of CMEC from 70% (fresh) to 69% (recycled) was observed. The low catalytic activity of the recycled Zr/ZIF-8 catalyst may be ascribed to formation of carbonaceous materials during the cycloaddition reaction as previously reported by Yuan et al. [72]. Furthermore, the XRD and FT-IR analyses results confirmed that Zr/ZIF-8 maintained its crystallinity throughout the reaction process.

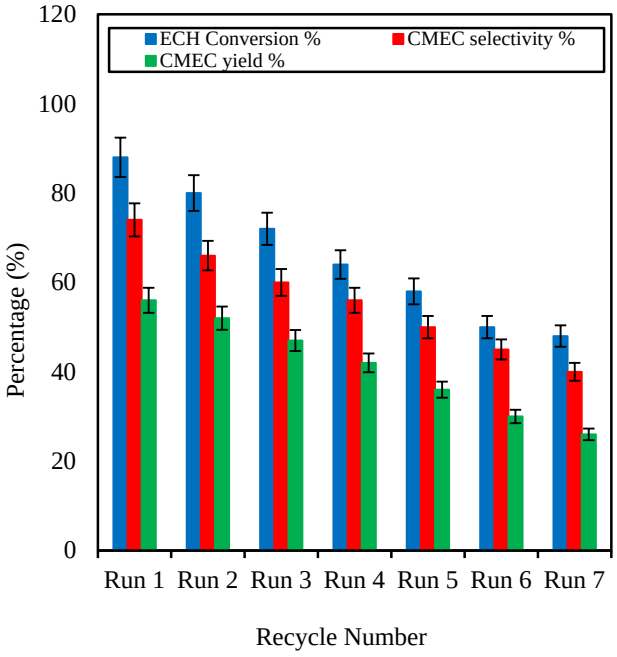

(**a**) **ZIF-8**

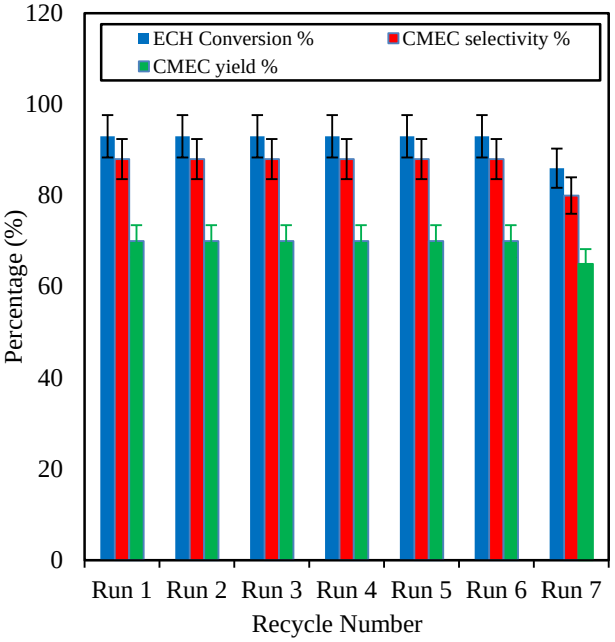

(**b**) **Zr/ZIF-8**

Figure 17. Catalyst reusability studies on conversion of ECH, selectivity and yield of CMEC. Experimental conditions: catalyst: (**a**) ZIF-8 and (**b**) Zr/ZIF-8; catalyst loading 10% (*w*/*w*); temperature 353 K; CO_2 pressure 8 bar; reaction time 8 h; stirring speed 350 rpm.

5. Conclusions

Zr/ZIF-8 has been successfully designed and assessed as a greener and highly efficient CO_2-reduction catalyst for the synthesis of CMEC. Although ZIF-8 is criticized by many researchers as thermally unstable for the synthesis of organic carbonates from CO_2 and epoxide, however, our

experiments have confirmed that the introduction of zirconium into ZIF-8 could strengthen the weak functionality, making it tenable for large-scale industrial applications. Several authors have utilized zirconium to reinforce different kinds of MOF experiments in order to achieve optimum results. However, their attempts have been unsatisfactory, partly because a firm balance between the required percentage of zirconium dopant and their host molecules was not established for those particular experiments. It may also be worth mentioning that this work has utilized a 10% dopant of zirconium for such a tremendous catalytic activity of Zr/ZIF-8. The stability tests carried out on both samples show that Zr/ZIF-8 demonstrates higher stability compared with single metal ZIF-8.

It has been concluded from the experimental results that there is a direct relationship between variation in the reaction conditions and ECH conversion, CMEC yield, and selectivity. From the experimental results, it can be observed that Zr/ZIF-8 catalyst displayed high epoxide conversions and high selectivity to chloromethyl ethylene carbonate at 353 K, without using any solvent or co-catalyst. Lewis acid copper (II) sites in the ZIF-8 frameworks promote adsorption of CO_2 on the solid surface and its further conversion to CMEC. The activity of reused Zr/ZIF-8 catalyst showed consistent stability over seven subsequent runs. The optimum reaction condition for the experiments was found at 353 K, 8 bar CO_2 pressure, and 8 h using fresh 10% (*w/w*) Zr/ZIF-8 catalyst loading for this reaction. Therefore, the development of a novel Zr/ZIF-8 catalyst for the synthesis of CMEC from CO_2 and ECH provided an efficient and promising greener route for CO_2 utilization.

Author Contributions: B.O.: main author and prepared the original draft. B.S.: Reviewed manuscript, gave comments, edited contents and supervised PhD student. All authors have read and agreed to the published version of the manuscript.

Funding: This research received no external funding.

Acknowledgments: Bisi Olaniyan is immensely grateful to the School of Engineering, LSBU, UK for partial financial assistance rendered throughout this research work.

Conflicts of Interest: The authors declare no conflict of interest.

References

1. Dai, W.L.; Luo, S.L.; Yin, S.F.; Au, C.T. The direct transformation of carbon dioxide to organic carbonates over heterogeneous catalysts. *Appl. Catal. A Gen.* **2009**, *366*, 2–12. [CrossRef]
2. Saada, R.; AboElazayem, O.; Kellici, S.; Heil, T.; Morgan, D.; Lampronti, G.I.; Saha, B. Greener synthesis of dimethyl carbonate using a novel tin-zirconia/graphene nanocomposite catalyst. *Appl. Catal. B Environ.* **2018**, *226*, 451–462. [CrossRef]
3. Baj, S.; Krawczyk, T.; Jasiak, K.; Siewniak, A.; Pawlyta, M. Catalytic coupling of epoxides and CO_2 to cyclic carbonates by carbon nanotube-supported quaternary ammonium salts. *Appl. Catal. A Gen.* **2014**, *488*, 96–102. [CrossRef]
4. Adeleye, A.I.; Kellici, S.; Heil, T.; Morgan, D.; Vickers, M.; Saha, B. Greener synthesis of propylene carbonate using graphene-inorganic nanocomposite catalysts. *Catal. Today* **2015**, *256*, 347–357. [CrossRef]
5. Onyenkeadi, V.; Kellici, S.; Saha, B. Greener synthesis of 1,2-butylene carbonate from CO_2 using graphene-inorganic nanocomposite catalyst. *Energy* **2018**, *165*, 867–876. [CrossRef]
6. Kathalikkattil, A.C.; Babu, R.; Tharun, J.; Roshan, R.; Park, D.W. Advancements in the Conversion of Carbon Dioxide to Cyclic Carbonates Using Metal Organic Frameworks as Catalysts. *Catal. Surv. Asia* **2015**, *19*, 223–235. [CrossRef]
7. Karagiaridi, O.; Lalonde, M.B.; Bury, W.; Sarjeant, A.A.; Farha, O.K.; Hupp, J.T. Opening ZIF-8: A catalytically active zeolitic imidazolate framework of sodalite topology with unsubstituted linkers. *J. Am. Chem. Soc.* **2012**, *134*, 18790–18796. [CrossRef]
8. Beyzavi, M.H.; Stephenson, C.J.; Liu, Y.; Karagiaridi, O.; Hupp, J.T.; Farha, O.K. Metal Organic Framework-Based Catalysts: Chemical Fixation of CO_2 with Epoxides Leading to Cyclic Organic Carbonates. *Front. Energy Res.* **2015**, *2*, 1–10. [CrossRef]
9. Rimoldi, M.; Howarth, A.J.; Destefano, M.R.; Lin, L.; Goswami, S.; Li, P.; Hupp, J.T.; Farha, O.K. Catalytic Zirconium/Hafnium-Based Metal-Organic Frameworks. *ACS Catal.* **2017**, *7*, 997–1014. [CrossRef]

10. Zhang, X.; Zhang, X.; Johnson, J.A.; Chen, Y.S.; Zhang, J. Highly Porous Zirconium Metal-Organic Frameworks with β-UH_3-like Topology Based on Elongated Tetrahedral Linkers. *J. Am. Chem. Soc.* **2016**, *138*, 8380–8383. [CrossRef]
11. Jeong, H.-M.; Roshan, R.; Babu, R.; Kim, H.-J.; Park, D.-W. Zirconium-based isoreticular metal-organic frameworks for CO_2 fixation via cyclic carbonate synthesis. *Korean J. Chem. Eng.* **2017**, *35*, 438–444. [CrossRef]
12. Yang, X.; Qiu, L.; Luo, X. ZIF-8 derived Ag-doped ZnO photocatalyst with enhanced photocatalytic activity. *RSC Adv.* **2018**, *8*, 4890–4894. [CrossRef]
13. Bai, Y.; Dou, Y.; Xie, L.-H.; Rutledge, W.; Li, J.-R.; Zhou, H.-C. Zr-based metal–organic frameworks: Design, synthesis, structure, and applications. *Chem. Soc. Rev.* **2016**, *45*, 2327–2367. [CrossRef] [PubMed]
14. Marshall, R.J.; Forgan, R.S. Postsynthetic Modification of Zirconium Metal-Organic Frameworks. *Eur. J. Inorg. Chem.* **2016**, *2016*, 4310–4331. [CrossRef]
15. Jin, Z.; Yang, H. Exploration of Zr–Metal–Organic Framework as Efficient Photocatalyst for Hydrogen Production. *Nanoscale Res. Lett.* **2017**, *12*, 850–854. [CrossRef] [PubMed]
16. Cavka, J.H.H.; Jakobsen, S.; Olsbye, U.; Guillou, N.; Lamberti, C.; Bordiga, S.; Lillerud, K.P.P. A New Zirconium Inorganic Building Brick Forming Metal Organic Frameworks with Exceptional Stability. *J. Am. Chem. Soc.* **2008**, *130*, 13850–13851. [CrossRef]
17. Jiang, M.; Cao, X.; Liu, P.; Zhang, T.; Zhang, J. ZIF-8@Polyvinylpyrrolidone Nanocomposites Based N-Doped Porous Carbon for Highly Efficient Oxygen Reduction Reaction in Alkaline Solution. *J. Electrochem. Soc.* **2016**, *163*, H459–H464. [CrossRef]
18. Gong, Q.; Luo, H.; Cao, D.; Zhang, H.; Wang, W.; Zhou, X. Efficient cycloaddition reaction of carbon dioxide with epoxide by Rhodamine based catalyst under 1 atm pressure. *Bull. Korean Chem. Soc.* **2012**, *33*, 1945–1948. [CrossRef]
19. Demir, S.; Usta, S.; Tamar, H.; Ulusoy, M. Solvent free utilization and selective coupling of epichlorohydrin with carbon dioxide over zirconium metal-organic frameworks. *Microporous Mesoporous Mater.* **2017**, *244*, 251–257. [CrossRef]
20. Schejn, A.; Aboulaich, A.; Balan, L.; Falk, V.; Lalevée, J.; Medjahdi, G.; Aranda, L.; Mozet, K.; Schneider, R. Cu^{2+}-doped zeolitic imidazolate frameworks (ZIF-8): Efficient and stable catalysts for cycloadditions and condensation reactions. *Catal. Sci. Technol.* **2015**, *5*, 1829–1839. [CrossRef]
21. Thi Thanh, M.; Vinh Thien, T.; Thi Thanh Chau, V.; Dinh Du, P.; Phi Hung, N.; Quang Khieu, D. Synthesis of Iron Doped Zeolite Imidazolate Framework-8 and Its Remazol Deep Black RGB Dye Adsorption Ability. *J. Chem.* **2017**, *2017*, 5045973. [CrossRef]
22. Sakakura, T.; Kohno, K. The synthesis of organic carbonates from carbon dioxide. *Chem. Commun.* **2009**, *2*, 1312–1330. [CrossRef] [PubMed]
23. Al-Janabi, N.; Hill, P.; Torrente-Murciano, L.; Garforth, A.; Gorgojo, P.; Siperstein, F.; Fan, X. Mapping the Cu-BTC metal-organic framework (HKUST-1) stability envelope in the presence of water vapour for CO_2 adsorption from flue gases. *Chem. Eng. J.* **2015**, *281*, 669–677. [CrossRef]
24. Coşkun, S.; Taşçi, Z.; Ulusoy, M.; Yurdakoç, M. Catalytic conversion of carbon dioxide into cyclic carbonates by Cu(II) and Ni(II) acetylacetonates anchored onto Siral 80. *Turk. J. Chem.* **2014**, *38*, 600–610. [CrossRef]
25. Saada, R. Catalytic Conversion of Carbon Dioxide (CO_2) into Value Added Chemicals. Ph.D. Thesis, London South Bank University, London, UK, 2015.
26. Gallardo-Fuentes, S.; Contreras, R.; Isaacs, M.; Honores, J.; Quezada, D.; Landaeta, E.; Ormazábal-Toledo, R. On the mechanism of CO_2 electro-cycloaddition to propylene oxides. *J. CO_2 Util.* **2016**, *16*, 114–120. [CrossRef]
27. Nabipour, H.; Sadr, M.H.; Bardajee, G.R. Synthesis and characterization of nanoscale zeolitic imidazolate frameworks with ciprofloxacin and their applications as antimicrobial agents. *New J. Chem.* **2017**, *41*, 7364–7370. [CrossRef]
28. Fan, G.; Zheng, X.; Luo, J.; Peng, H.; Lin, H.; Bao, M.; Hong, L.; Zhou, J. Rapid synthesis of Ag/AgCl@ZIF-8 as a highly efficient photocatalyst for degradation of acetaminophen under visible light. *Chem. Eng. J.* **2018**, *351*, 782–790. [CrossRef]
29. Nordin, N.A.H.M.; Ismail, A.F.; Mustafa, A. Synthesis and preparation of asymmetric PSf/ZIF-8 mixed matrix membrane for CO_2/CH_4 separation. *J. Teknol. (Sci. Eng.)* **2014**, *69*, 73–76. [CrossRef]
30. Zhu, M.; Srinivas, D.; Bhogeswararao, S.; Ratnasamy, P.; Carreon, M.A. Catalytic activity of ZIF-8 in the synthesis of styrene carbonate from CO_2 and styrene oxide. *Catal. Commun.* **2013**, *32*, 36–40. [CrossRef]

31. Da Silva, J.D.S.F.; Malo, D.L.; Bataglion, G.A.; Eberlin, M.N.; Ronconi, C.M.; Alves, S.; De Sá, G.F. Adsorption in a fixed-bed column and stability of the antibiotic oxytetracycline supported on Zn(II)-[2-methylimidazolate] frameworks in aqueous media. *PLoS ONE* **2015**, *10*, 1371–1381.
32. Fang, Q.-R.; Makal, T.A.; Young, M.D.; Zhou, H.-C. Recent Advances in the Study of Mesoporous Metal-Organic Frameworks. *Comments Inorg. Chem.* **2010**, *31*, 165–195. [CrossRef]
33. Panchariya, D.K.; Rai, R.K.; Anil Kumar, E.; Singh, S.K. Core-Shell Zeolitic Imidazolate Frameworks for Enhanced Hydrogen Storage. *ACS Omega* **2018**, *3*, 167–175. [CrossRef] [PubMed]
34. Liu, J.; He, J.; Wang, L.; Li, R.; Chen, P.; Rao, X.; Deng, L.; Rong, L.; Lei, J. NiO-PTA supported on ZIF-8 as a highly effective catalyst for hydrocracking of Jatropha oil. *Sci. Rep.* **2016**, *6*, 1–11. [CrossRef] [PubMed]
35. Na, L.Y.; Hua, R.N.; Ning, G.L.; Ou, X.X. Nano/Micro HKUST-1 Fabricated by Coordination Modulation Method at Room Temperature. *Science* **2012**, *28*, 555–558.
36. Goyal, S.; Shaharun, M.S.; Kait, C.F.; Abdullah, B. Effect of monometallic copper on zeolitic imidazolate framework-8 synthesized by hydrothermal method. *J. Phys. Conf. Ser.* **2018**, *1123*, 6. [CrossRef]
37. Cychosz, K.A.; Guillet-Nicolas, R.; García-Martínez, J.; Thommes, M. Recent advances in the textural characterization of hierarchically structured nanoporous materials. *Chem. Soc. Rev.* **2017**, *46*, 389–414. [CrossRef]
38. Yin, H.; Kim, H.; Choi, J.; Yip, A.C.K. Thermal stability of ZIF-8 under oxidative and inert environments: A practical perspective on using ZIF-8 as a catalyst support. *Chem. Eng. J.* **2015**, *278*, 293–300. [CrossRef]
39. North, M.; Pasquale, R.; Young, C. Synthesis of cyclic carbonates from epoxides and CO_2. *Green Chem.* **2010**, *12*, 1514–1539. [CrossRef]
40. Zanon, A.; Chaemchuen, S.; Mousavi, B.; Verpoort, F. 1 Zn-doped ZIF-67 as catalyst for the CO_2 fixation into cyclic carbonates. *J. CO_2 Util.* **2017**, *20*, 282–291. [CrossRef]
41. Pang, S.H.; Han, C.; Sholl, D.S.; Jones, C.W.; Lively, R.P. Facet-specific stability of ZIF-8 in the presence of acid gases dissolved in aqueous solutions. *Chem. Mater.* **2016**, *28*, 6960–6967. [CrossRef]
42. Zhou, K.; Mousavi, B.; Luo, Z.; Phatanasri, S.; Chaemchuen, S.; Verpoort, F. Characterization and properties of Zn/Co zeolitic imidazolate frameworks vs. ZIF-8 and ZIF-67. *J. Mater. Chem. A* **2017**, *5*, 952–957. [CrossRef]
43. Bosch, M.; Zhang, M.; Zhou, H. Increasing the Stability of Metal-Organic Frameworks. *Adv. Chem.* **2014**, *10*, 18232–28237. [CrossRef]
44. Xie, Y.; Wang, T.-T.; Liu, X.-H.; Zou, K.; Deng, W.-Q. Capture and conversion of CO_2 at ambient conditions by a conjugated microporous polymer. *Nat. Commun.* **2013**, *4*, 1960–1967. [CrossRef] [PubMed]
45. Zhou, L.; Li, N.; Owens, G.; Chen, Z. Simultaneous removal of mixed contaminants, copper and norfloxacin, from aqueous solution by ZIF-8. *Chem. Eng. J.* **2019**, *362*, 628–637. [CrossRef]
46. Yao, J.; He, M.; Wang, K.; Chen, R.; Zhong, Z.; Wang, H. High-yield synthesis of zeolitic imidazolate frameworks from stoichiometric metal and ligand precursor aqueous solutions at room temperature. *CrystEngComm* **2013**, *15*, 3601–3606. [CrossRef]
47. Giraldo, L.; Barranco, M.B.; Húmpola, P.; Carlos, J.; Piraján, M. the adsorption of phenols derivatives in aqueous solution. *J. Chem.* **2017**, *8*, 6940–6949.
48. Song, Q.; Nataraj, S.K.; Roussenova, M.V.; Tan, J.C.; Hughes, D.J.; Li, W.; Bourgoin, P.; Alam, M.A.; Cheetham, A.K.; Al-Muhtaseb, S.A.; et al. Zeolitic imidazolate framework (ZIF-8) based polymer nanocomposite membranes for gas separation. *Energy Environ. Sci.* **2012**, *5*, 8359–8366. [CrossRef]
49. Luanwuthi, S.; Krittayavathananon, A.; Srimuk, P.; Sawangphruk, M. In situ synthesis of permselective zeolitic imidazolate framework-8/graphene oxide composites: Rotating disk electrode and Langmuir adsorption isotherm. *RSC Adv.* **2015**, *5*, 46617–46623. [CrossRef]
50. Mao, J.; Ge, M.; Huang, J.; Lai, Y.; Lin, C.; Zhang, K.; Meng, K.; Tang, Y. Constructing multifunctional MOF@rGO hydro-/aerogels by the self-assembly process for customized water remediation. *J. Mater. Chem. A* **2017**, *5*, 11873–11881. [CrossRef]
51. Biswal, B.P.; Shinde, D.B.; Pillai, V.K.; Banerjee, R. Stabilization of graphene quantum dots (GQDs) by encapsulation inside zeolitic imidazolate framework nanocrystals for photoluminescence tuning. *Nanoscale* **2013**, *5*, 10556–10561. [CrossRef]
52. Tanaka, S.; Fujita, K.; Miyake, Y.; Miyamoto, M.; Hasegawa, Y.; Makino, T.; Van Der Perre, S.; Cousin Saint Remi, J.; Van Assche, T.; Baron, G.V.; et al. Adsorption and Diffusion Phenomena in Crystal Size Engineered ZIF-8 MOF. *J. Phys. Chem. C* **2015**, *119*, 28430–28439. [CrossRef]

53. Pham, T.T.; Le, L.N.; Nguyen, H.N.; Luong, T.T.K.; Pham, T.N.; Nguyen, H.L.; Nguyen, T.K. Encapsulating gold nanoparticles in zeolitic imidazolate framework crystal for novel optical response. *Polyhedron* **2018**, *148*, 171–177. [CrossRef]
54. Wang, S.; Ma, Z.; Du, X.; Zhang, S.; Chen, Z. Lanthanum doping of metal-organic frameworks-5 and its effect on thermal stability and CO_2 adsorption property. *Mater. Express* **2018**, *8*, 381–387. [CrossRef]
55. Li, P.Z.; Wang, X.J.; Liu, J.; Lim, J.S.; Zou, R.; Zhao, Y. A Triazole-Containing Metal-Organic Framework as a Highly Effective and Substrate Size-Dependent Catalyst for CO_2 Conversion. *J. Am. Chem. Soc.* **2016**, *138*, 2142–2145. [CrossRef] [PubMed]
56. Abhang, R.M.; Wani, K.S.; Patil, V.S. Synthesis and Characterization of ZIF-8 Filler for Preparation of Mixed Matrix Membrane. *Int. J. Sci. Eng. Res.* **2015**, *6*, 1276–1280.
57. Adeleye, A.I. Heterogeneous Catalytic Conversion of Carbon Dioxide to Value Added Chemicals. Ph.D. Thesis, London South Bank University, London, UK, June 2015.
58. Kim, H.U.; Babu, R.; Roshan, R.; Park, D.W. Catalytic performance of metal azolate frameworks in the solventless synthesis of cyclic carbonates from CO_2 and epoxides. *Appl. Catal. A Gen.* **2017**, *538*, 59–65. [CrossRef]
59. Kim, J.; Kim, S.N.; Jang, H.G.; Seo, G.; Ahn, W.S. CO_2 cycloaddition of styrene oxide over MOF catalysts. *Appl. Catal. A Gen.* **2013**, *453*, 175–180. [CrossRef]
60. Wang, M.; She, Y.; Zhou, X.; Ji, H. Efficient solvent-free synthesis of chloropropene carbonate from the coupling reaction of CO_2 and epichlorohydrin catalyzed by magnesium porphyrins as chlorophyll-like catalysts. *Chin. J. Chem. Eng.* **2011**, *19*, 446–451. [CrossRef]
61. Onyenkeadi, V.; Aboelazayem, O.; Saha, B. Systematic multivariate optimisation of butylene carbonate synthesis via CO_2 utilisation using graphene-inorganic nanocomposite catalysts. *Catal. Today* **2019**, *3*, 1–13. [CrossRef]
62. Saada, R.; Kellici, S.; Heil, T.; Morgan, D.; Saha, B. Greener synthesis of dimethyl carbonate using a novel ceria-zirconia oxide/graphene nanocomposite catalyst. *Appl. Catal. B Environ.* **2015**, *168–169*, 353–362. [CrossRef]
63. Liang, J.; Chen, R.-P.; Wang, X.-Y.; Liu, T.-T.; Wang, X.-S.; Huang, Y.-B.; Cao, R. Postsynthetic ionization of an imidazole-containing metal–organic framework for the cycloaddition of carbon dioxide and epoxides. *Chem. Sci.* **2017**, *8*, 1570–1575. [CrossRef] [PubMed]
64. Adeleye, A.I.; Patel, D.; Niyogi, D.; Saha, B. Efficient and greener synthesis of propylene carbonate from carbon dioxide and propylene oxide. *Ind. Eng. Chem. Res.* **2014**, *53*, 18647–18657. [CrossRef]
65. Sathe, A.A.; Nambiar, A.M.; Sturgis, N.; Rioux, M. Synthesis of cyclic organic carbonates via catalytic oxidative carboxylation of olefins in flow reactors. *Catal. Sci. Technol.* **2017**, *7*, 2–3. [CrossRef]
66. Dhakshinamoorthy, A.; Asiri, A.M.; Garcia, H. Metal-organic frameworks as heterogeneous catalysts in liquid phase reactions: Why are they so exceptional? *Chim. Oggi-Chem. Today* **2015**, *33*, 40–45.
67. Mousavi, B.; Chaemchuen, S.; Phatanasri, S.; Chen, C.; Zeng, C.; Ganguly, R.; Zhuiykov, S.; Verpoort, F. Selective cyclodimerization of epichlorohydrin to dioxane derivatives over MOFs. *Arab. J. Chem.* **2017**, *10*, 1878–1888. [CrossRef]
68. Maeda, C.; Miyazaki, Y.; Ema, T. Recent progress in catalytic conversions of carbon dioxide. *Catal. Sci. Technol.* **2014**, *4*, 1482–1489. [CrossRef]
69. Carreon, M.A. Metal organic frameworks as catalysts in the conversion of CO_2 to cyclic carbonates. *Indian J. Chem.—Sect. Inorg. Phys. Theor. Anal. Chem.* **2012**, *51*, 1306–1314.
70. Miralda, C.M.; MacIas, E.E.; Zhu, M.; Ratnasamy, P.; Carreon, M.A. Zeolitic imidazole framework-8 catalysts in the conversion of CO_2 to chloropropene carbonate. *ACS Catal.* **2012**, *2*, 180–183. [CrossRef]
71. De Caro, P.; Bandres, M.; Urrutigoïty, M.; Cecutti, C.; Thiebaud-Roux, S. Recent progress in synthesis of glycerol carbonate and evaluation of its plasticizing properties. *Front. Chem.* **2019**, *7*, 1–13. [CrossRef]
72. Yuan, S.; Zou, L.; Li, H.; Chen, Y.P.; Qin, J.; Zhang, Q.; Lu, W.; Hall, M.B.; Zhou, H.C. Flexible Zirconium Metal-Organic Frameworks as Bioinspired Switchable Catalysts. *Angew. Chem. —Int. Ed.* **2016**, *55*, 10776–10780. [CrossRef]